Optimal Channel Selection for Improved Classification Accuracy in fNIRS BCI

Author: Aakif Mehboob

Regn Number: 00000204605

Supervisor

Dr. Muhammad Jawad Khan

DEPARTMENT OF ROBOTICS AND ARTIFICIAL INTELLIGENCE

SCHOOL OF MECHANICAL & MANUFACTURING ENGINEERING

NATIONAL UNIVERSITY OF SCIENCES AND TECHNOLOGY

ISLAMABAD

NOVEMBER 2020

Optimal Channel Selection for Improved Classification Accuracy in fNIRS BCI

Author: Aakif Mehboob

Regn Number: 00000204605

A thesis submitted in partial fulfillment of the requirements for the degree of

MS Robotics and Intelligent Machine Engineering

Thesis Supervisor:

Dr. Muhammad Jawad Khan

Thesis Supervisor's Signature: _____

DEPARTMENT OF ROBOTICS AND ARTIFICIAL INTELLIGENCE

SCHOOL OF MECHANICAL & MANUFACTURING ENGINEERING

NATIONAL UNIVERSITY OF SCIENCES AND TECHNOLOGY,

ISLAMABAD

NOVEMBER 2020

Declaration

I certify that this research work titled "*Optimal Channel Selection for Improved Classification Accuracy in fNIRS BCI"* is my own work. The work has not been presented elsewhere for assessment. The material that has been used from other sources it has been properly acknowledged / referred.

Signature of Student
AAKIF MEHBOOB
00000204605

Plagiarism Certificate (Turnitin Report)

This thesis has been checked for Plagiarism. Turnitin report endorsed by Supervisor is attached.

Signature of Student
AAKIF MEHBOOB
Reg Number: 00000204605

Signature of Supervisor
DR. MUHAMMAD JAWAD KHAN

Copyright Statement

Acknowledgements

‘In the name of Allah the most Beneficent and the most Merciful’

All praises to the creator of whole universe, Almighty Allah Subhana-hu Wa-ta’ala, without his will nothing is possible. I am deeply humbled and thankful to my Allah that you have made it possible for me to achieve this milestone in my life. You have definitely eased this journey for me and You have definitely made completion of my work fluently.

I am profoundly thankful to my family for their continuous encouragement, support, care and prayers. My parents unparalleled love, sacrifices and appropriate direction for building up strong foundation for education helped me finish countless endeavors in my life. The consistent uplift, support and inspiration provided by my wife and children helped me in completion of this degree.

I would like to express special thanks to my supervisor and my teacher Dr. Muhammad Jawad Khan for steering me in the right way and imparting his knowledge in this study. I am also thankful for courses which he has taught me and I can safely say that I haven't learned any other engineering subject in such depth than the ones which he has taught. I would like to pay my sincerest regards and appreciation to my teacher and mentor Dr. Noman Naseer for his guidance, direction and suggestions in every area of this research. I would like to express my gratitude to Dr. Yasar Ayaz and Dr. Hasan Sajid for being on my thesis guidance and evaluation committee and I would like to pay my acknowledgement for their help and expertise.

I would also like to pay utmost recognition to my dearest friend Syed Hammad Nazeer Gilani for his assistance and cooperation throughout my MS degree. Each time I got stuck in something, he came up with the solution. Without his sincere help and contributions I wouldn’t have been able to complete my thesis. I would profusely appreciate his patience and guidance for this entire work.

Finally, I would like to thank all my friends, colleagues, class fellows and peers who contributed in each and every aspect of my work and rendered valuable input into my study.

Dedicated to my parents especially my late father, my wife and children, for their tremendous support and cooperation throughout this endeavor that led me to this wonderful accomplishment.

Abstract

Functional near-infrared spectroscopy (fNIRS) is a portable non-invasive modality used excessively in modern brain computer interface (BCI) systems with ultimate goal of aiding people suffering from temporary or permanent disabilities. The brain data acquired using fNIRS devices is associated with the user intentions through mental activation and then, decoded into control commands. Classification accuracy is one of the measures of state-of-the-art BCI systems, identifying region of interest (ROI) or channel of interest (COI) and optimal channel selection may enhance classification performance. Effectiveness of fNIRS-BCI can be substantially increased by selecting cortical activity based channel selection methods. This research is aimed at selection of optimal channels for fNIRS-BCI system by proposing z-score method to improve classification accuracy. In the proposed method, cross correlation technique is applied between acquired brain signal and desired hemodynamic response function (dHRF). The z-scores of maximum values of correlation coefficients for each channel are calculated and channels showing positive z-scores are selected for further processing. Comparative analysis of the proposed method is done with already existing *t*-value method and it is further validated by calculating classification accuracies without channel selection technique i.e. using all channels. The study utilizes open access dataset that contained brain signals of 17 healthy subjects for a two-class fNIRS-BCI problem (task vs rest); right-hand finger tapping (RFT), left-hand finger tapping (LFT) and foot tapping (FT). Conventional statistical features i.e. mean, peak, slope, skewness, kurtosis and variance of the oxygenated hemoglobin (HbO) signal were used as features for classification by linear discriminant analysis (LDA). The classification accuracies achieved by using the proposed method for RFT vs rest, LFT vs rest, and FT vs rest tasks were 72.24 ± 6.2%, 72 ± 8.1% and 69.41 ± 6.7%, respectively. The results yielded by the z-score method have shown a considerable improvement in classification performance as a step forward for performance enhancement for BCI systems.

Key Words: *functional Near Infra-Red Spectroscopy, Brain Computer Interface, z-score method, Cross Correlation, t-*value *method, Channel selection, Channel of interest*

Table of Contents

List of Figures

List of Tables

CHAPTER 1: INTRODUCTION

This chapter presents in detail discussion about Brain Computer Interface (BCI) and its different stages, different modalities being used in BCI focusing mainly on function Near Infrared Spectroscopy (fNIRS), identifying the gap areas and scope of this research work.

1.1 Background

Brain Computer Interface (BCI), also known sometimes as Brain Machine Interface (BMI) is a method that generates control commands using brain signals for establishing an interface or link between brain and external devices by bypassing the involvement of muscles or peripheral nerves [1]. BCI provides an alternate channel for messages or brain signals to interact with external world. The main purpose of BCI is to serve as a rehabilitation tool for people suffering from motor disabilities (amputations, paralysis, Amyotrophic Lateral Sclerosis, Locked in syndrome disease, spinal cord injury etc). It can be used by impaired persons to control peripheral devices like prosthetic limb, wheel chair, computer etc. to interact and communicate with their surroundings. The overall theme of working of BCI system is shown in Figure 1.1.

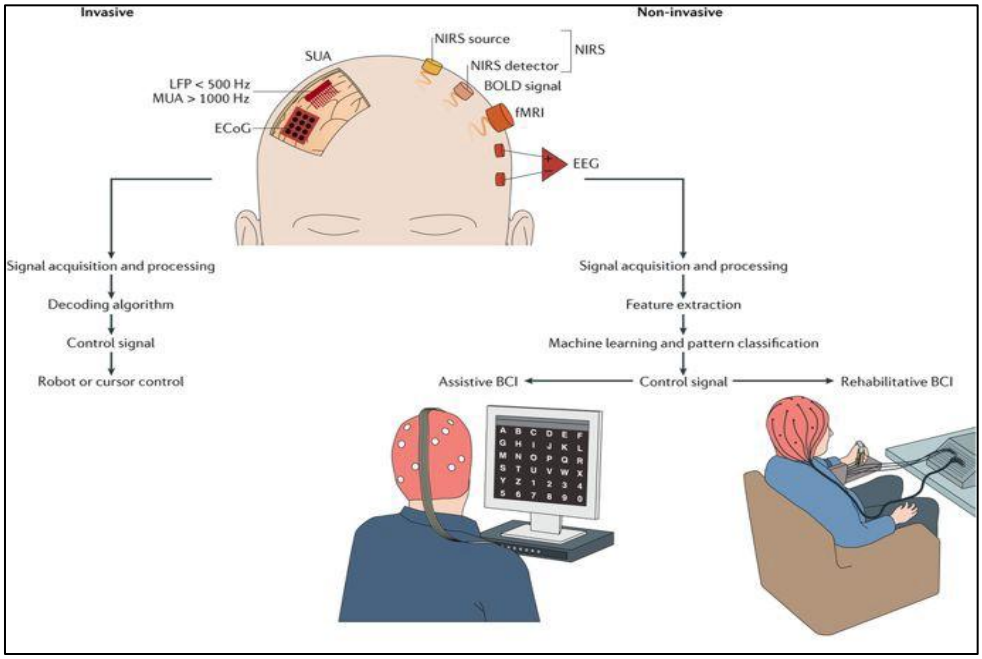

Figure 1.1: Brain Computer Interface (BCI) overview and its modalities (Chaudhary et al. 2016 [2])

There mainly exist three approaches in BCI systems for detecting neural activity i.e. invasive BCI, semi-invasive BCI, and non-invasive BCI. The invasive method, also known as intracortical neuron recording, requires surgical procedures in brain to implant the micro-electrode array inside cortex. This method acquires signal with very high spatial resolution and Signal-to-Noise Ratio (SNR) which resultantly provides accurate neuro-prosthetic control with multiple degree of freedoms [3], [4]. In semi-invasive BCI, the placement of electrode mesh is done beneath the skull and on the surface of cortex through craniotomy. Electrocorticography (ECoG), is a semi-invasive modality, that gathers electrical signals directly from cortex by means of the said placed electrodes. ECoG also receives a better signal in terms of SNR and spatial resolution as compared to non-invasive approaches like Electroencephalography (EEG). Although both invasive and semi-invasive modalities receive significantly better and less noisy brain signals, however it possesses major health risk due to involvement of surgery. The anatomical or technical issues that may arise in these methods are bio-compatability of implanted electrodes with brain tissues, potential risk of infection due to involvement of wireless hardware and failure of system or tissue damage due to continuous switching of equipment. Therefore both of these approaches prove to be less viable and a short term solution.

Contrary to the abovementioned two modalities, there exists a non-invasive method for which no surgical procedures are required. This type of BCI system uses wearable devices mounted on surface of the scalp. Non-invasive BCI is widely used in research for being clinically safe and often provides portable solutions. It also acquires relatively more type of brain signals for further processing [2]. Nevertheless the downsides of non-invasive modalities are that it acquires weaker signal with low spatial resolution as compared to its counterparts. Electroencephalography (EEG), functional near-infrared spectroscopy (fNIRS), functional magnetic resonance imaging (fMRI) and magnetoencephalography (MEG) are typical non-invasive BCI modalities currently used for research purposes. However, fNIRS and EEG are most frequently utilized for having several advantages like ease of accessibility, affordability, portability and offering flexibility for customizing different experimental paradigm.

Due to the usefulness and easiness of non-invasive modalities, these are most commonly used in research field. However, these modalities have some advantages and disadvantages in

comparison to one another. Each of non-invasive modality is discussed here with their pros and cons. MEG, is type of non-invasive modality, measures magnetic field resulting from the flow of electric currents in the neurons. Its advantages include lower distortion due to skull & scalp and higher spatiotemporal resolution as compared to EEG. Therefore, it offers less training time, faster response and reliable communication channel. In spite of all these benefits, MEG device is too expensive and requires specialized shielded room maintaining environmental conditions (Figure 1.2). Due to which MEG is very often used and is practically less useful for everyday use. EEG records electrophysiological brain signals, by placing electrodes on the scalp (Figure 1.3), which arise due to electrical neuron firings caused as a result of mental activity in the cortical area. This is the most commonly used modality in the field of BCI for being inexpensive, safe and easily available. Because EEG signal is acquired from the scalp, it is of poor quality mixed with superficial noises. EEG offers good temporal resolution but it has very low spatial resolution.

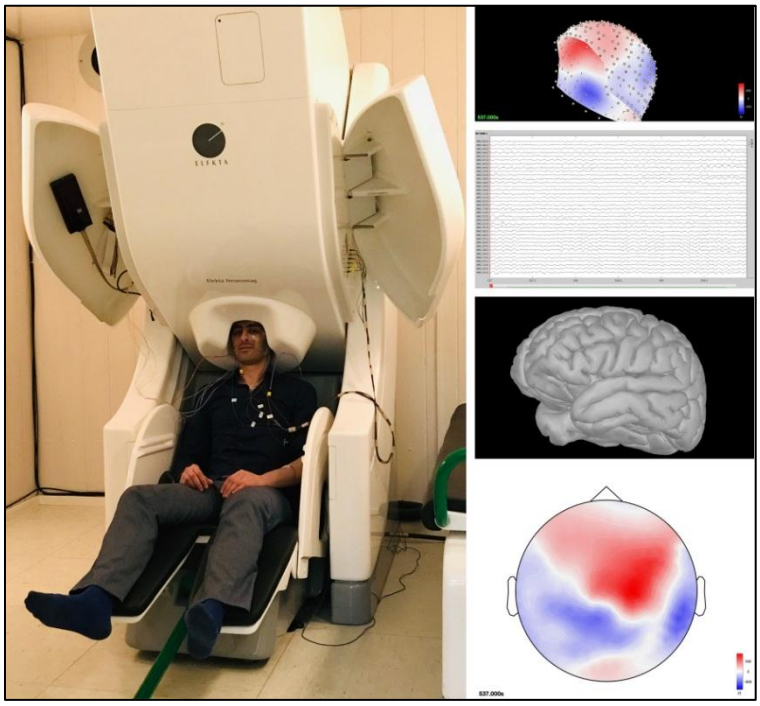

Figure 1.2: Magnetoencephalography (MEG) Scanner

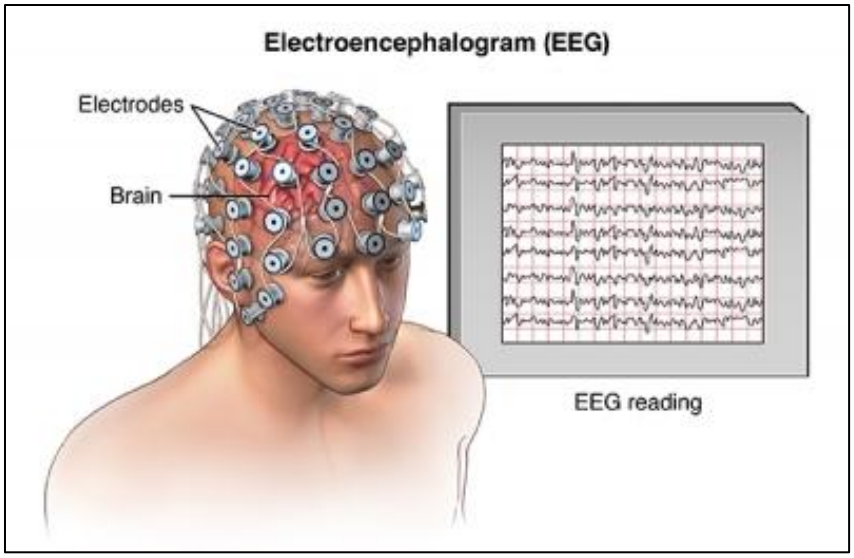

Figure 1.3: Electroencephalography (EEG)

The working principle of fMRI and fNIRS are almost similar in nature. fMRI detects the changes in blood oxygenation level, cerebral blood flow and volume through scanners that generates electromagnetic fields. These changes are linearly related to neuronal activity, therefore it is indirect method of measuring cortical activation. It usually measures the Blood Oxygenation Level Dependent (BOLD) signal resulting due to metabolic activity inside brain. Like MEG scanners, fMRI devices are also cumbersome (Figure 1.4) and expensive making it less practical for normal applications. fMRI offers very good spatial resolution because of which it is very useful in localizing active brain regions. However, due to delay in response time it has low temporal resolution and is also sensitive to motion artifacts.

Figure 1.4: fMRI Scanner

fNIRS is relatively new and emerging neuroimaging modality being used in BCI (Figure 1.5). Similar to fMRI, it measures concentration changes in blood oxygenation level and cerebral blood flow due to neural activity in brain or local capillary network through Near Infra-Red (NIR) light. As penetrating depth of NIR light is limited to 1-3 cm, due to which it can measure metabolic activity in outer cortical layer of brain. Its advantages include its compact size, portability, simplicity, low cost and having reasonable temporal resolution. However, it has low spatial resolution and due to anatomical constraint localization of active brain region is difficult. fNIRS signal is corrupted by motion artifacts and physiological noises that includes heart beats, respiration and Mayer waves.

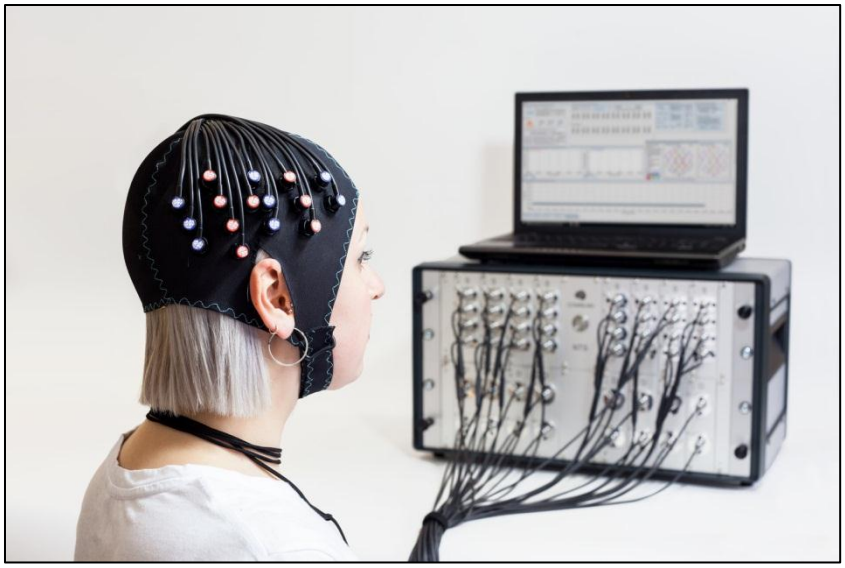

Figure 1.5: fNIRS device

BCI can also be classified, based on the stimulation technique, into two types. It can be exogenous or endogenous. If the stimulus is evoked by some external means either visually or auditory, it is called exogenous BCI. But endogenous BCI type does not require any external stimulus to generate brain potentials. Through constant training and feedback, user might be able to produce specific type of brain rhythms. This type has the advantage of self-generation of signals and control of devices at free will. On the other hand, exogenous type of BCI user is constrained to respond to specific type of choices presented to him.

Another categorization of BCI is asynchronous and synchronous BCI based on the processing of input signals. In synchronous BCI, a predefined experimental protocol is followed in which only those signals are selected that lies within specified timeframe. This has an advantage of being aware of the activation period of brain well in advance and nullifying the possibility of unusual signals like physiological noises or motion artifacts in that time window. While in asynchronous BCI, monitoring of brain signals are carried out continuously independent of any cue based stimulus. This type is also known as self-paced as user can decide when to control the external devices.

BCI can also be classified into three types with respect to Human-Computer Interaction (HCI) [5]. These types are Active, Reactive and Passive BCI. The Active BCI is a direct and independent method for controlling interfaces or devices by generating user intentions without any external aid. Like in case of motor imagery, the signals are generated through motor cortex by visualizing the movements of specific body part in absence of any actual movements. While in Reactive BCI, external stimulus is required for controlling the output that is indirectly generated by user. An example of this is mental arithmetic, in which user calculate numbers based on what flashes on screen in front of him. Another example is acupuncture that generates its output as a reaction to external stimulation i.e. insertion of needle at Hegu points. Last one is Passive BCI, in which brain activity is acquired without any voluntary control commands by user, contrary to other two methods. In this type user is not required to perform any task. Passive BCI is usually used for assessing mental state of user or sometimes it is required for improving HCI.

In order to effectively use brain signal for controlling external devices, it has to go through five stages i.e. Signal acquisition, Pre-processing, feature extraction, classification and application interface [6] as depicted in Figure-1.6. First of all brain signal is acquired by appropriate means using suitable devices placed on entire or specific brain region based on relative mental activity. Any of the aforementioned modality can be used keeping in view the suitability and ease for user. The most common brain areas used for acquiring brain signals are pre-frontal and primary motor cortices. Motor cortex generates signals that corresponds to activities like motor imagery and motor execution, while pre-frontal signals corresponds to music imagery, landscape imagery, mental arithmetic and mental counting etc. The study by Hong et al. (2018) [7] showed that total 13 types of activities can be performed and detected using prefrontal cortex.

In second stage, i.e. the Pre-processing stage, different sort of noises in the signal like experimental, instrumental & physiological noises are removed by applying suitable filters or other methods. These noises arise due to system hardware, experimental setup, motion artifacts, external interferences, heart beats, respiration and blood pressure. Low pass filter is mostly used to remove instrumental noises because of its high frequency. Experimental noises are usually

removed by methods like Principal Component Analysis (PCA) based filtering, Wiener filtering, wavelet analysis and Savitzky-Golay filters. And for removal of physiological noises methods like Independent Component Analysis (ICA), PCA, adaptive filtering and band-pass filtering are used.

After pre-processing of signal, appropriate features are extracted and selected. It is crucial to select appropriate features for generating commands that result in high classification accuracy. The features are generally characterized into three types i.e. spatial, temporal and spatio-temporal features [7]. The most widely used heuristic features for EEG and fNIRS-BCI are signal mean, peak, slope, variance, kurtosis, skewness, zero-crossing, latency and power spectrum density. Some researchers have also used Genetic Algorithms for finding combination of optimal feature sets. Other commonly used features for EEG-BCI are logarithm power band, and Common Spatial Pattern (CSP).

Afterwards, classification algorithms are applied on extracted features for identification of activities that are later used as commands for application interface. The classifiers, by implementing supervised learning techniques, are first trained and validated and then are able to detect mental activity in testing phase. Some of most common classifiers that are implemented are Linear Discriminant Analysis (LDA), Support Vector Machine (SVM), Artificial Neural Network (ANN), Hidden Markov Model (HMM) etc.

Finally, the applications of BCI include neuro-rehabilitation, motor restoration, communication and other etc. BCI can be helpful for patients with cerebrovascular diseases like stroke to regain and restore motor functions through manipulation or self-regulation of neural activity. Patients suffering from Locked-in Syndrome (LIS), Amyotrophic Lateral Sclerosis (ALS) diseases or spinal cord injury are unable to communicate freely with outside world. In that case, BCI is used as a mean of communication by decoding mental choices, controlling cursors or alphanumeric grids. BCI is also applied in assisting patients with motor disabilities, for example paralysis or amputations, by controlling wheel chair, robotic arm or prosthetic limb. Other applications of BCI include environment control, gaming and entertainment purposes.

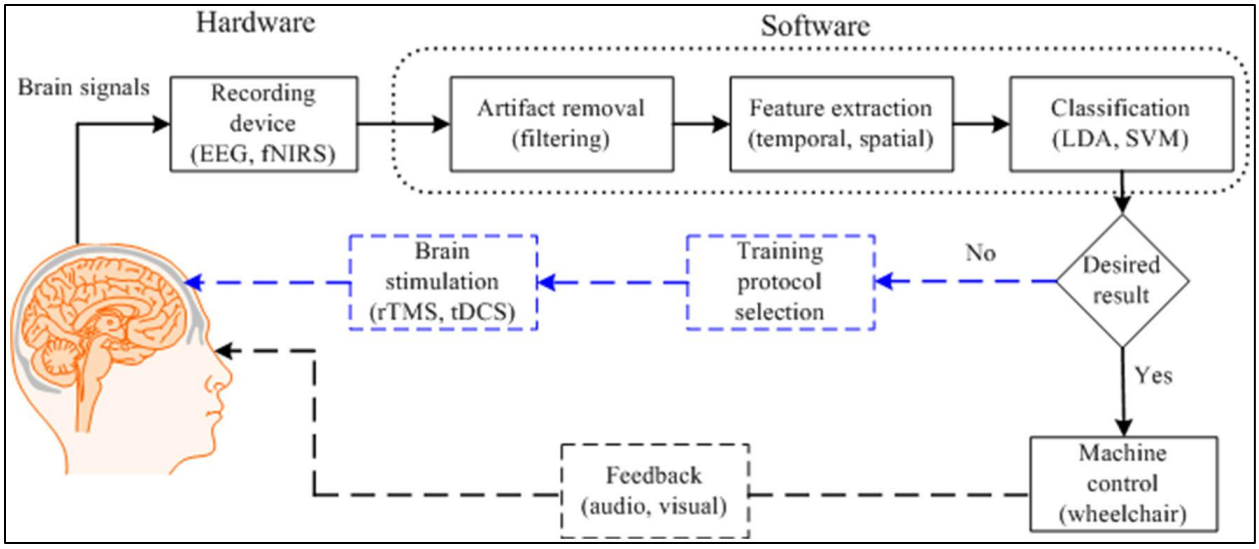

Figure 1.6: Schematic of a Typical BCI system (Hong et al. 2018 [7])

1.2 Scope

The scope of this thesis includes fNIRS-BCI and a focused and detailed discussion on fNIRS has been covered. fNIRS is a relatively a new technology and its experimentation was first reported to be performed in 1977 by Jobsis [8]. In field of BCI, its first implementation was done in 2004 by Coyle [9]. It uses optical method (Near Infra-Red light ~ 650-1000 nm wavelength) to detect changes in concentration of oxygenation in hemoglobin (main chromophore). fNIRS exhibits slow response time due to shallow penetration of NIR light into skull and in-built delays of hemodynamic response. In spite of that, it is considered feasible modality for BCI because of it is portable, non-invasive, and economical and offers relatively reasonable temporal resolution.

fNIRS devices mainly operate in near-infrared spectrum (650 – 1000nm) and NIR light has the capability to penetrate into scalp, skull and brain tissues. Whenever a mental activity is performed, due to requirement of energy an increase in oxygen consumption and regional cerebral blood flow is resulted. The said intravascular activity in brain region is indirectly detected through NIR light by calculating changes in oxygen level of blood chromophores i.e. oxygenated hemoglobin (HbO) and deoxygenated hemoglobin (HbR). Since fNIRS is an optical imaging modality, it consists of sources (LED, Laser diode) and detectors (Photo diode, Avalanche photo diode, Photomultiplier tube) and each pair of source-detector forms a channel.

The sources emit NIR light of multiple wavelengths (02 or more) that penetrate through scalp, skull and brain tissues where it is either absorbed or scattered multiple times. Some of these photons are reflected back, exiting brain layers and are detected by different detectors placed on the scalp. These detectors acquire the raw optical intensity resulting from incident illuminations.

Because of multiple scattering and absorptions of NIR light by chromophores, the strength of illuminated light is reduced. The said variations in optical intensities are converted into respective changes in HbO and HbR by using using Modified Beer Lambert Law (MBLL) [10]. The method is an indirect way of detecting neuronal activity in blood capillary network and brain through HbO & HbR. The cortical activations causes increase in HbO, cerebral blood volume and regional cerebral blood flow and simultaneous decrease in HbR. As the mental activity tends to finish, rise in HbR and fall in HbO concentrations are observed.

Three types of fNIRS measurement techniques exists namely continuous wave (CW), frequency domain (FD) and time domain (TD). CW type modality illuminates light continuously at fixed intensity and receive back attenuated signal with the help of detectors. In FD technology, modulated intensity light is emitted and received back along with phase shift. While TD technique emits light intensity of extremely short duration (usually in form of pulses) and subsequently measure the shape of pulse.

Usually, brain signal in fNIRS is extracted from two of the most commonly used brain regions i.e. Pre-Frontal Cortex (PFC) and Primary Motor Cortex (PMC). Motor execution, motor imagery and other motor related tasks are associated to PMC while PFC corresponds to intuitive and logical tasks like music imagery, mental counting, mental arithmetic and landscape imagery etc. Placement of the device on one or both of the aforementioned brain areas depends on specific type of mental task that needs to be performed.

1.3 Problem Statement

By using larger section of brain region gives an advantage of extracting multiple numbers of control commands for application interface. However, increase in number of control commands is compromised by lower classification accuracy. Also, in order to keep optimal

separation distance (in fNIRS devices) between source & detector i.e. 3 – 5 cm [11], [12] optodes cannot be increased beyond a certain number. The downsides of using larger number of channels is that it is computationally complex, time consuming and inconvenient for subjects.

Signal acquisition by using multi-channel device can cover larger area of brain and consequently give better performance of signals. In order to find the functionally active area of brain, determination of region of interest (ROI) / channel of interest (COI) is indispensable. Furthermore, some channels contain irrelevant or redundant information that is undesirable and may result into lower classification accuracy. The data on these redundant channels can be avoided to save computational cost and achieve better classification accuracy with fewer channels. In practical scenarios as well it is considered viable to use as minimum channels as possible.

In this thesis, cross correlation method is applied between acquired cortical signal and desired hemodynamic response. Afterwards, z-scores of the obtained correlation coefficients are calculated and positive z-scores define the active channels. Subsequently, optimal channels is determined which resulted in better classification accuracy by curtailing the un-desired channels. Previously conducted studies that have implemented channel selection methods are covered in literature review section. The proposed method for channel selection used in this study and conventional *t*-value method is discussed in Materials and Methods section. The results obtained through are discussed in detail with comparison to the already existing method. Finally, the research is concluded and future research work is proposed in conclusion section.

CHAPTER 2: LITERATURE REVIEW

As discussed in the introduction chapter that BCI system consist of five stages that includes signal acquisition, pre-processing, feature extraction, classification and application interface. There exists another step prior feature extraction stage, which is selection of active brain region, also known as Region of Interest (ROI). In field of medical imaging, ROI is the region that contains diagnostic information and is selected for further study in order to correctly identify the disease. In fMRI, specific region exhibits specific functionality among different brain regions from where the useful signal can be extracted. Sometimes it seems necessary to explore underlying signal from entire brain through ROI. ROI analysis is useful in finding activation across different variables and conditions, it also helpful in decreasing number of statistical tests and hence reducing type-I error and additionally to remain specified to smaller areas for limited test / trials [13]. In fNIRS context, the channels that belong to a specific ROI show considerable increase in hemodynamic response in comparison to baseline measurement as a result of applied stimulus.

In fNIRS devices, there are limited numbers of optodes and it's usually placed on head at specified positions. Therefore, it is very challenging to know exactly that the placed optodes are correctly translating accurate ROI. Usually 10-20 system is being used for placement of optodes, however Jurcak et al. (2007) have also implemented 10-10 and 10-5 systems in addition to 10-20 system for enhancing spatial resolution [14]. Morais et al. (2018) developed a toolbox that automatically places the fNIRS optodes at predefined positions based on 10-10 and 10-5 systems [15].

Recently, bundled optode configurations have been used to precisely identify the active regions of the brain [16], [17]. This method is involved in Spatially Resolved Spectroscopy (SRS) and used for brain imaging of active regions. Nguyen and Hong (2016) used densely placed optodes for improving the spatial resolution of fNIRS [17]. It consisted of 02 scans and in 1^{st} scan the active local brain region was identified with 12 channels placed on pre-frontal cortex. In 2^{nd} scan, bundled optode arrangement with 256 channels was used on active region for in-depth analysis and brain imaging. In another work by Nguyen [16], bundled optode electrodes were used, however active channels in ROI were determined by *t*-value method.

Another approach is to divide optodes placed on specific brain region into local sub-regions and finding out the most active sub-region amongst all by averaging over local region. During offline training stage the local sub-region is selected and afterwards it is used during testing stage. Khan & Hong (2015) [18] applied the same approach on 28 channels, placed on prefrontal cortex (PFC) and dorsolateral prefrontal cortex (DPFC), by dividing them into three sub-regions named as A (1-8 channels), B (9-20 channels) and C (21-28 channels). Their results showed that sub-region A was most active amongst the three separated regions. Although this method reduces overall number of channels by rejecting inactive regions, however there is a chance that the active sub-region may contain unwanted channels.

Apart from hardware based approaches, there are few algorithms that have been applied w.r.t. channel selection for fNIRS devices. The methods that have been applied are *t*-value method, baseline correction method, cross-correlation and other techniques. The *t*-value method finds out the statistical significance, by fitting the evoked response to the desired response, of estimated coefficients [16], [19]. The *t*-value is the ratio of weighting coefficients to its standard error and its positive ($t>0$) or threshold value ($t>t_{crt}$, where t_{crt} depends on degree of freedom) decides whether the channel data is significant or not. Santosa et al. (2014) [19] firstly applied this method in his study for selection of hemodynamic responses having positive *t*-values. In another study by Hong & Santosa (2016) [20], *t*-value method was used for detection of ROI against different sound stimulus by placing optodes on both right and left hemisphere. The channels that give *t*-values greater than threshold value of 1.6736 were selected. It is worth mentioning here that different channels against different subjects and stimulus were obtained. This shows that activation of channels is not uniform among different subjects due to variation in physical structure of brain. Similarly, specific task is associated to a certain brain region that's why identification of correct ROI is extremely important. As mentioned earlier, Nguyen et al. (2016) [16] also used *t*-value method for selection of active channels in the bundled optode configuration placed on left motor cortex. The criteria for selection was set as $t>1.66$ and $p<0.05$ in accordance with degree of freedom and significance level, respectively. The *t*-value method is explained in detail in Materials and Methods chapter.

In another approach, the maximum values during rest and corresponding task states are compared for selection of active channels and is known as baseline correction method. If the maximum value during task period is higher than maximum value in rest period then channel is termed as active and used for further processing. If the value is negative then the channel is discarded. Khan & Hong (2017) [21] have applied this method for selection of active channels in hybrid EEG-fNIRS BCI and decoded eight commands for quad copter control. Although, this method of selection is easy and computationally inexpensive but it may result in higher variation.

Rojas et al. (2016) [22] have applied cross correlation method for identification of potential dominant channel in both hemisphere and found out its relationship with neighboring channels in pain related cortical activations. Through visual inspection the potential dominant channel was verified then by calculation in delay of response the neighboring active channels were identified. Similarly in another study by Rojas et al. (2016) [23], potential dominant channels in ROI were identified that shows fastest and strongest activations. Then using cross correlation the effects on neighboring channels were computed and it was re-evaluated through optical flow analysis.

Kovelman et al. (2008) [24] used PCA to identify channels in ROI and MRI coregistration was applied to verify location of active channels against hypothesized location. Li et al. (2017) [25] used General Linear Model (GLM) for selection of most significant single fNIRS channel and its adjacent EEG electrode in each hemisphere for hybrid EEG-fNIRS BCI system. In another hybrid fNIRS-EEG study, Kwon et al. (2020) [26] applied sequential backward selection algorithm and determined 02 EEG channels and 02 fNIRS source-detector (SD) pair. Ge. et al (2017) [27] selected suitable EEG and fNIRS channels though source analysis and spatial locations of cortical activations for bimodal EEG-fNIRS BCI system.

Although placement of large number of sensors increases the number of channels and identification of active region is enhanced. However, large number of channels may contain redundant information and sometimes may have unwanted data. Also, the more channels there are the more difficult it is to post-process and analyze the brain signal data, thereby increasing computational complexity. Therefore, there is need to correctly identify the bare minimum

number of channels that contain useful data for further improving processing time, reducing complicated analysis and ultimately enhancing classification accuracy.

In this thesis, cross correlation method is applied between a modeled hemodynamic response function and acquired data from different channels from which maximum of the correlation coefficients are extracted. The most significant correlation coefficients are selected based on its z-score ($z>0$), which shows active channels. In comparison to proposed method, channel selection was applied using conventional *t*-value method. Further validation is performed using all channels i.e. without any channel selection technique. Classification accuracies were calculated using z-score selected channels, *t*-value selected channels and all channels.

As discussed above, the channel selection algorithms have been explored by researchers before, though it is difficult to draw a comparison between each algorithm with respect to suitability and effectiveness of the methods. It is worth mentioning here that, as cross correlation method for channel selection have been used earlier [22], [23], however the proposed method is applied with different approach and technique. Furthermore, in previous studies [22], [23] the scope of BCI was not covered. Notwithstanding above, the ultimate goal of channel selection in all methods is to reduce the complexity and enhancing the accuracies of fNIRS BCI systems. The same is the objective of this study.

Table 2.1: Review of recently used channel selection techniques in fNIRS-BCI systems

References	Cortical Activity / Cortical region	BCI	Modality	Channel selection methods	Selected Channels	Total channels	Accuracy
Kovelman et al. (2008) [24]	Broca's area and Verbal Working Memory (Attention Prefrontal Cortex Area)	No	fNIRS	Principal Component Analysis	5	24	N/A
Hu et al. (2013) [28]	Resting state and Right hand finger tapping (Motor Cortex)	No	fNIRS	Seed based correlation method	11	34	N/A
Rojas et al. (2016a) [23]	Pain related activity / Acupuncture (somatosensory cortex)	No	fNIRS	Cross correlation	6-10	24	N/A
Rojas et al. (2016b) [22]	Pain related activity / Acupuncture	No	fNIRS	Cross correlation	6-9	24	N/A

	(somatosensory cortex						
Nguyen et al. (2016) [17]	Right little & thumb finger movements (Left motor cortex)	No	fNIRS	*t*-value method (t>0)	Not specified	48	N/A
Hong & Santosa (2016) [20]	Auditory cortex using four sound categories	Yes	fNIRS	*t*-value method (t>1.6736)	14 (English) 13 (annoying) 5(non-english) 4 (nature)	44	73.0 ± 10.23%, 70.9 ± 11.05%
Khan et al. (2017) [21]	Mental Arithmetic, Mental Counting, Mental rotation, word formation, eye blinks and eye movements (PFC for fNIRS & PMC for EEG)	Yes	EEG-fNIRS	Baseline correction method	2-10	16	76.5 % ± 11.3
Ge et al. (2017) [27]	Motor Imagery tasks (Primary Motor Cortex)	Yes	EEG-fNIRS	Source analysis of brain activation	3 EEG 10 fNIRS	64 EEG 31 fNIRS	56.8% (fNIRS) 74.7% (EEG) 81.2% (Hybrid)
Li et al. (2017) [25]	Motor Execution task (Primary Motor Cortex)	Yes	EEG-fNIRS	General Linear Model (GLM)	2 fNIRS 2 EEG	34 fNIRS 14 EEG	85.55% (fNIRS) 85.64% (EEG) 91.02% (Hybrid)
Kwon et al. (2020) [26]	Mental arithmetic, Right hand motor imagery, Idle State (motor and prefrontal cortices)	Yes	EEG-fNIRS	Sequential Backward Selection	2 EEG 2 fNIRS SD pairs	21 EEG 16 fNIRS	77.6 ± 12.1%

CHAPTER 3: MATERIALS AND METHODS

In this chapter the precise conduct of experiment and algorithms that have been applied in current research are covered in detail. The chapter is sub-divided into two sections that include materials section and methods section. In each section stepwise explanation is given about the entire setup and techniques applied to achieve the desired results.

3.1 Materials

The materials section describes about the subjects that have participated in experiments, device being used, experimental setup and protocol to acquire the desired brain signal. The details are ensued in following sub-sections.

3.1.1 Participants

Open access dataset [29] have been utilized in this thesis containing unilateral finger tapping (Right and left hand fingers tapping) and foot tapping for 2-class classification; i.e. task vs rest. Seventeen healthy subjects (right handed, 23.4 ± 2.5 years old) participated in the experiment. None of the subject had any history of neurological or psychiatric disorder that could have affected the experiment. The participants were briefed about the experiment in detail and written consent was also recorded before performing data acquisition. All the experimentation was performed in accordance with latest ethical codes given in declaration of Helsinki.

3.1.2 Experimental Setup

Multi-channel continuous-wave fNIRS device (LIGHTNIRS, Shimadzu, Kyoto, Japan) with triple-wavelengths semiconductor lasers (780, 805 and 830 nm), with sampling frequency of 13.33 Hz, was used for signal acquisition. The setup consists of total eight light sources and eight detectors. Four of each sources and detectors were placed around C3 and C4 on left and right hemisphere respectively of motor cortex area. Separation of 3cm was maintained between each source and detector. The placement of optodes and location of channels is shown in Figure 3.1.

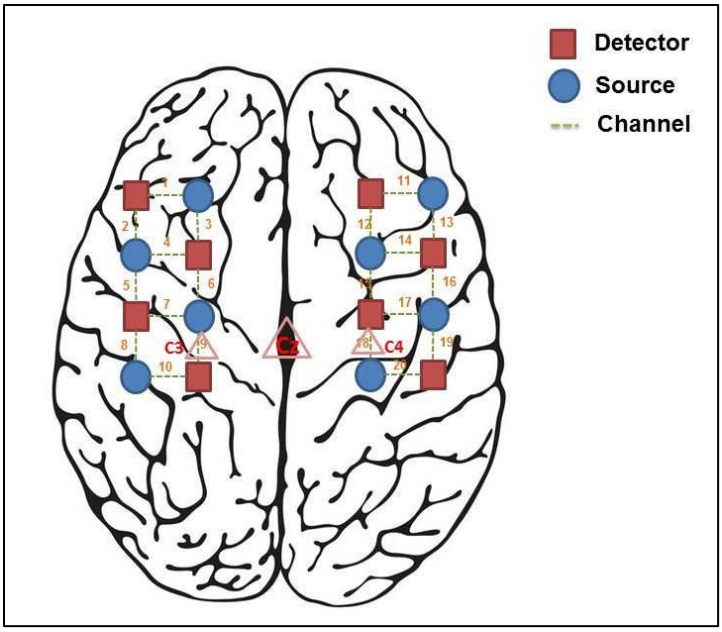

Figure 3.1: fNIRS optodes placement and channels location on motor cortex region. Ch 1-10 lies on left hemisphere region near C3 (Ch-9) area while Ch 11-20 lies on right hemisphere region near C4 (Ch-18).

3.1.3 Experimental Paradigm

The experiment was carried out in a quiet room and participants were seated on a comfortable chair. Complete set of instructions and information related to the experiment were displayed on a 27 inch monitor placed in front of them. The experimental session consisted of three tasks i.e. right hand finger-tapping (RHT), left hand finger-tapping (LFT) and foot tapping (FT) conducted in three separate sessions. Each task session comprised of 25 trials and single trial consist of 2 sec introduction period and 10 sec task period followed by inter trial rest period of 17-19 sec. The triggers were marked in a data file transmitted at the initiation of task period and specific type of task was displayed randomly to the participants. At the start of each task a short beep is generated and subjects are required to perform assigned task continuously in the task period. The inter trial rest period is also triggered through short beep along with display of 'STOP' sign on the monitor. In the RHT and LHT tasks, unilateral complex finger tapping was performed by participants. They were instructed to tap their thumbs with other fingers sequentially starting from index to little finger and then in reverse order. The tapping of fingers was repeatedly continued at a rate of almost 2 Hz. In FT task the foot on the same dominant hand side was tapped constantly at 1 Hz. The experimental paradigm is depicted in Figure 3.2.

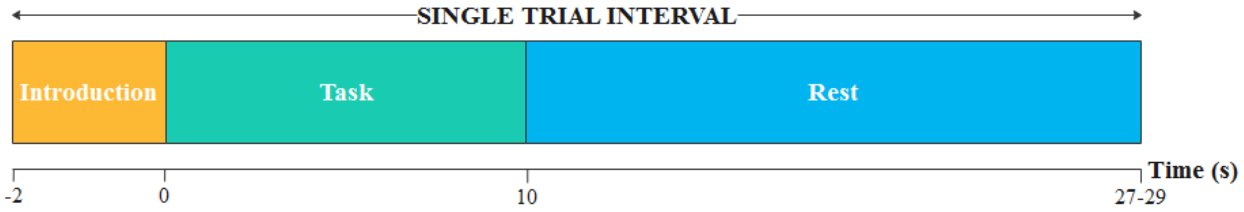

Figure 3.2: Experimental paradigm followed in all three tasks i.e. RHT, LHT and FT. Single trial interval consisted of initial rest period of 2s, then task period of 10s and at the end inter-trial rest state of 17-19s.

3.2 Methods

In this section, all the techniques and algorithms that have been applied after the acquisition of signals to generate binary control commands are explained in detail. The methods that convert raw optical signal into relative oxygen concentrations and pre-processing techniques for removal of different noises are explained in 'Signal acquisition and Processing'. The channel selection algorithms applied i.e *t*-value method and proposed z-score method are discussed in 'Channel Selection'. The features and classifiers being used in current study are explained in 'Feature Extraction' and 'Classification' sections, respectively. The overall methodology is depicted in Figure 3.3.

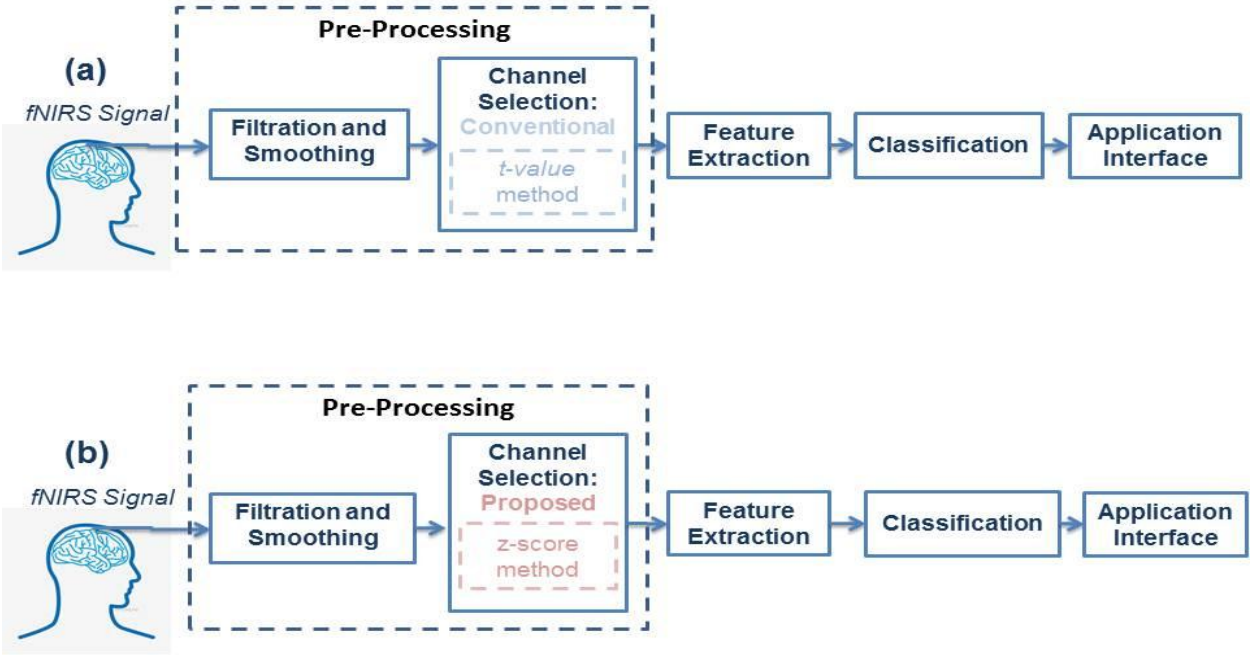

Figure 3.3: The process flow of methodology (a) with *t*-value method and (b) proposed z-score method

3.2.1 Signal Acquisition and Processing

As discussed earlier, concurrent concentration changes in HbO and HbR due to evoked stimulus are measured through Modified Beer Lambert Law (MBLL) [10]. The dual wavelength signals are used for the purpose of finding out two unknown variables HbO and HbR. The device used in the existing setup consisted of three wavelengths which is helpful in finding 3rd unknown variable i.e. total hemoglobin (HbT) level. However, values of HbO and HbR are only calculated using two wavelengths in the current study. The Beer Lambert Law, from which MBLL has been deduced, deals with intensity calculation in non-scattering media. The illustration of light entering and exiting from a medium without any scatter is given below:

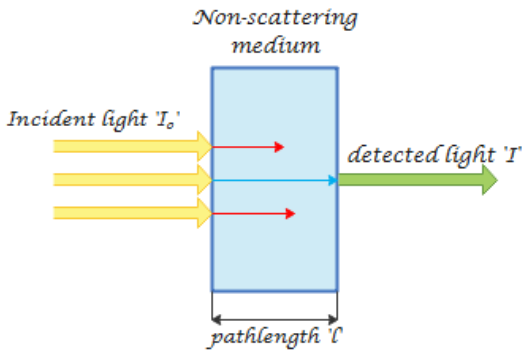

Figure 3.4: Phenomenon of light entrance (I_o) and exit (I) from a non-scattering medium with pathlength of 'l'. The red arrows show the absorption of light and blue arrow shows the travel of light without any scatter

In that case, the Beer Lambert Law equation is:

$$I(t) = I_0(t)e^{-\mu_a \times l} \tag{3.1}$$

Where I(t) and $I_0(t)$ is the detected and transmitted light at time 't', respectively. 'μ_a' is the absorption coefficient and 'l' is the pathlength or source-detector distance. However, in actual scenario light doesn't travel in straight path, there is geometrical factor 'G' and scattering in the human tissues are involved. Additionally, the path of light traveled is not straight line and hence a differential path length is also incorporated in above equation. Considering these factors the equation becomes:

$$I(t) = I_0(t)e^{-(\mu_a + \mu_s) \times l \times d + G} \tag{3.2}$$

Where, 'μ_s' is the scattering coefficient and 'G' is factor that is associated with measurement geometry. '$d(\lambda_i)$' is the differential path length factor that is dependent upon μ_s and μ_a. By rearranging above equation and taking natural log on both sides, it becomes:

$$A\,(t,\lambda_i) = -ln\frac{I(t)}{I_0(t)} = \,(\mu_a + \,\mu_s) \times l \times d(\lambda_i) + G \tag{3.3}$$

The term 'A' is the absorbance in the medium (also known as optical density) and since it is ratio of light intensities, it is unitless. Absorbance 'A' is both time 't' and wavelength 'λ_i' (i=1,2 for two wavelengths) dependent. In MBLL it is assumed that loss due to scattering is constant and absorption in tissue is changed homogenously. Also the concentration changes are measured instantaneously so the geometrical factor is assumed to be negligible.

$$A\,(t,\lambda_i) = \,\mu_a(t,\lambda_i) \times l \times d(\lambda_i) \tag{3.4}$$

Since the optical density 'A' is measured at two time instances, 't_1' is the incident time and 't_2' is the time of detection. Also the term 'μ_a' can be decomposed into two components; i.e. molar extinction coefficient '$\Delta\alpha_{HbX}$' and concentration changes 'ΔC_{HbX}' of chromophores. Therefore the above equation becomes:

$$\mu_a(t,\lambda_i) = [\alpha_{HbO}(\lambda_i)\Delta C_{HbO}(t) \,+\, \alpha_{HbR}(\lambda_i)\Delta C_{HbR}(t)] \tag{3.5}$$

$$\Delta A\,(t,\lambda_i) = [\alpha_{HbO}(\lambda_i)\Delta C_{HbO}(t) \,+\, \alpha_{HbR}(\lambda_i)\Delta C_{HbR}(t)] \times l \times d(\lambda_i) \tag{3.6}$$

The units of '$\Delta\alpha_{HbX}$' and 'ΔC_{HbX}' are $\mu M^{-1}mm^{-1}$ and μM, respectively. By calculating the equation (3.6) at two wavelengths 'λ_1' and 'λ_2', we are able to find the two unknown concentration changes (ΔC_{HbO} & ΔC_{HbR}) in the tissue.

$$\Delta A\,(t,\lambda_1) = [\alpha_{HbO}(\lambda_1)\Delta C_{HbO}(t) \,+\, \alpha_{HbR}(\lambda_1)\Delta C_{HbR}(t)] \times l \times d(\lambda_1) \tag{3.7}$$

$$\Delta A\,(t,\lambda_2) = [\alpha_{HbO}(\lambda_2)\Delta C_{HbO}(t) \,+\, \alpha_{HbR}(\lambda_2)\Delta C_{HbR}(t)] \times l \times d(\lambda_2) \tag{3.8}$$

By rearranging equations (3.7) and (3.8), we are able to calculate concentration changes of HbO & HbR [$\Delta C_{HbO}(t)$ & $\Delta C_{HbR}(t)$]:

$$\begin{bmatrix}\Delta C_{HbO}(t)\\ \Delta C_{HbR}(t)\end{bmatrix} = \begin{bmatrix}\alpha_{HbO}(\lambda_1) & \alpha_{HbR}(\lambda_1)\\ \alpha_{HbO}(\lambda_2) & \alpha_{HbR}(\lambda_2)\end{bmatrix}^{-1}\begin{bmatrix}\Delta A(t,\lambda_1)/d(\lambda_1)\\ \Delta A(t,\lambda_2)/d(\lambda_2)\end{bmatrix} \times \frac{1}{l} \tag{3.9}$$

The calculated HbO and HbR signals are contaminated with different noises like experimental, instrumental and physiological noises. The experimental noises arise due to motion artifacts and sudden motions causes intensity variations resulting in noise spikes. Instrumental noises are mainly due to some high frequency components in the hardware or environmental effects. The physiological noises are due to respiration (0.2~0.5 Hz), heart beat (1~1.5 Hz), and mayer wavers (~0.1 Hz).

Firstly and fore-mostly the physiological noises in the signal are removed using 4^{th} order butterworth bandpass filter. The pass-band of the filter was selected between 0.03Hz to 0.15Hz so that abovementioned physiological noises are effectively removed and signal can be further processed. In order to smooth the HbO & HbR signals and remove noises due to motion artifacts Savitzky-Golay (SG) filter is used. This filter is basically used to smooth the input signal with the help of polynomial fitting on a moving window. SG filter is a finite impulse response (FIR) filter that smoothes signal by keeping the shape and peak heights of the original signal. It defines a symmetric filter which discretely replaces the input signal with the values that lies on the smooth polynomial curve.

Suppose that we have an input vector 'x' with N-dimensional length and we wish to fit into our signal a polynomial curve '$\hat{x}_m$' of dimensions 'd' having coefficients 'c_d'. Also assume that 'N' is odd and have 'M' data points on each side with 'x_0' as middle point i.e. N = 2M+1. Then we will have following set of equations:

$$x = [x_{-m}, x_{-m+1}, \cdots x_{-1}, x_0, x_1, \cdots\ x_{m-1}, x_m]^T \tag{3.10}$$

$$\hat{x}_m = \ c_0 + c_1 m + c_2 m^2 + \cdots + c_{d-1} m^{d-1}, c_d m^d; \ \ -M \leq m \leq M \tag{3.11}$$

And the polynomial basis vector 's_i' (i = 0,1, … ,d) with dimensions d+1, in equation and matrix form is given below:

$$s_i(m) = \ m^i; \ -M \leq m \leq M \tag{3.12}$$

$$S = [s_0, \ s_1, \ s_2, \cdots\cdots, s_d] \tag{3.13}$$

The polynomial vector '$\hat{x}$' in terms of coefficients and basis vector can be written as:

$$\hat{x} = \sum_{i=0}^{d} c_i \boldsymbol{s_i} = [s_0,\ s_1,\ \ \ldots,\ \ s_d] \begin{bmatrix} c_0 \\ c_1 \\ \vdots \\ c_d \end{bmatrix} = S\boldsymbol{c} \tag{3.14}$$

The main purpose of the above equations is to minimize mean square error ($e = \hat{x} - x$) and elaborative calculations are given in [30]. The summarized forms of equations are given below:

$$G = S(S^T S)^{-1} \equiv [g_0, g_1, \cdots, g_d] \tag{3.15}$$

$$B = SG^T = GS^T \equiv [b_{-M}, \cdots, b_0, \cdots, b_M] \tag{3.16}$$

In above equation, the columns of matrix B are SG filter set and '$\mathbf{b_0}$' is useful in sense that being central filter element it is used for further evaluation. The other important equations are of corresponding coefficient vector 'c_i' and smooth polynomial equation:

$$c_i = {g_i}^T x; \qquad i = 0, 1, ,2, \cdots, d \tag{3.17}$$

$$\hat{x}_m = {b_m}^T x; \qquad -M \le m \le M \tag{3.18}$$

So the middle smoothed value ($\hat{x}_0 = y_0$), that is actually required, is obtained through middle SG filter 'b_0' by putting m=0 in equation (3.18):

$$\hat{x}_0 = y_0 = {b_0}^T x = \sum_{m=-M}^{M} b_0(m) x_m \tag{3.19}$$

So the resulting Savitzky-Golay filter of order 'd', length of 'N', after shifting vector 'x' to the *n*th instant can be written as:

$$y(n) = \sum_{m=-M}^{M} b_0(m)\, x(n+m) = \sum_{m=-M}^{M} b_0(-m) x(n-m) \tag{3.20}$$

3.2.2 Channel Selection Methods

The channel selection algorithms that are used in this study are *t*-value method and proposed z-score method. Prior implementation of both the methods, one of the common step is to model canonical hemodynamic response function (cHRF). Hemodynamic response is a process caused by short and intense neural activation in blood capillaries of brain region. It has been discussed earlier that fNIRS device measure metabolic activity that is directly interlinked with neuronal activity. During stimulation, the active neurons of brain require energy which is

provided by glucose and oxygen in the blood. Hemoglobin molecule, which is an oxygen carrier in blood, becomes oxygenated (i.e. HbO) and travels in blood stream to the active area causing rise in HbO level. Subsequently, due to consumption of oxygen in activated area, concentration level of deoxygenated hemoglobin (HbR) increases with decrease in HbO. The HRF function, also known as cHRF, results from three factors i.e. consumption of oxygen, blood flow and blood volume. It consists of majorly three characteristics / components i.e. initial dip, peak and undershoot and the signal usually lasts from 20-30 sec as shown in Figure 3.5.

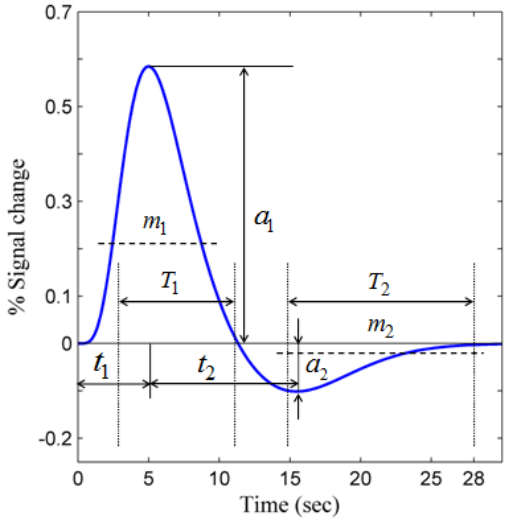

Figure 3.5: The typical cHRF response curve generated by two gamma functions. Where, a_1: Peak of response, a_2: Peak of undershoot, t_1: time to peak, t_2: time to undershoot, T_1: time of activation period, T_2: time of deactivation period, m_1: mean in T_1 and m_2: mean in T_2. [31]

There exist different methods to model cHRF function, which are two gamma functions, three gamma functions, basis function under GLM approach, sum of inverse logit functions, FIR based models, cHRF with temporal derivative and cHRF with dispersion derivative etc. But the most common out of all these models are two and three gamma functions. Formula for modeling cHRF using two gamma functions [32]–[34]is as under:

$$h_c(k) = A\left[\frac{k^{\alpha_1-1}\beta_1^{\alpha_1}e^{-\beta_1 k}}{\Gamma(\alpha_1)} - c\,\frac{k^{\alpha_2-1}\beta_2^{\alpha_2}e^{-\beta_2 k}}{\Gamma(\alpha_2)}\right] \tag{3.21}$$

The parameter 'A' sets the amplitude, 'α_1' & 'α_2' set delays of the peak and undershoot respectively, while 'β_1' & 'β_2' set dispersions of the peak and undershoot respectively, 'c' is ratio of the peak to the undershoot and 'Γ' is the gamma distribution. In order to model the cHRF with initial dip, three gamma functions [32] are used.

$$h_c(k) = \sum_{i=1}^{3} \left[A_i \frac{k^{\alpha_i - 1} \beta_i^{\alpha_i} e^{-\beta_i k}}{\Gamma(\alpha_i)} \right] \quad (3.22)$$

Similarly, for i=1 to 3, the parameters 'A' sets the amplitude, 'α' sets the delay, 'β' sets the rate dispersion for initial dip, peak and undershoot of hemodynamic response function. In this research, two gamma function (equation 3.21) has been applied with parameter values as A=1, α_1=6, α_2=16, β_1=β_2=1 and c=1/6 [33].

After modeling cHRF function, the modeled or desired hemodynamic response function (dHRF) is calculated by convolution cHRF i.e. $h_c(k)$ with boxcar function i.e. $s(k)$. Formulation is given as under:

$$h_M(k) = \sum_{n=0}^{k-1} h_c(n) s(k-n) \quad (3.23)$$

Where the boxcar function is given below:

$$s(k) = \begin{cases} 0, & if\ k \in rest \\ 1, & if\ k \in task \end{cases} \quad (3.24)$$

The boxcar function is basically a unit step function having value of '0' for rest period and '1' for task period.

_t_-value Method

Afterwards *t*-value or z-score methods are applied seperately. *t*-value method is an estimation based channel selection approach in which channels with positive *t*-value are selected. Alternatively, a threshold value of 't' (i.e $t > t_{crt}$) can also be set for selection of active channels. In that case, degree of freedom (N-1) is used to determine the value of threshold, where N is number of samples in an activity (N=373 in this case).

This channel selection approach determines the cortical activation through statistical estimation by fitting measured response to the linear regression model [19]. The said estimation can be calculated by fitting dHRF with measured hemodynamic response function that results from cortical activation. It can be formulated as given below:

$$h_j^i(k) = \phi_j^i h_M(k) + \psi_j^i . 1 + \varepsilon_j^i \quad (3.25)$$

The term on left side of the equation i.e. $h_j^i(k)\ \epsilon\ R^{N\ X\ 1}$ is the measured response function in which 'N' is the number of samples in each stimulus, subscript 'j' denotes the stimulus number, superscript 'i' denotes the channel number and 'k' is the stimulus type (i.e. k=0 is rest and k=1 is task in the stimulus). 'ϕ' is the unknown coefficient to be estimated, the coefficient 'ψ' is multiplied by column vectors of $1\ \epsilon\ R^{N\ X\ 1}$ for correction of baseline drift in the signal and $\varepsilon\ \epsilon\ R^{N\ X\ 1}$ the error term in the linear regression method. The unknown coefficients 'ϕ' are estimated through *robustfit()* function in MATLAB®.

After estimation of coefficient 'ϕ' by using the aforementioned model (equation 3.25), its statistical significance is calculated by ratio of the estimated coefficient and it's Standard Error (SE). The said statistical significance is also called '*t*-value'. Its positive or threshold value greater than critical value shows that channel is active or otherwise.

$$t_j^i = \frac{\phi_j^i}{SE\ (\phi_j^i)} \tag{3.26}$$

The above formula gives *t*-value in i-th channel of j-th stimulus. In this case, active channels are considered which have *t*-value greater than 't_{crt}', which is '1.66' (degree of freedom is 372 i.e. N-1). The method of channel selection using *t*-value can be depicted by flow chart as shown in Figure 3.6.

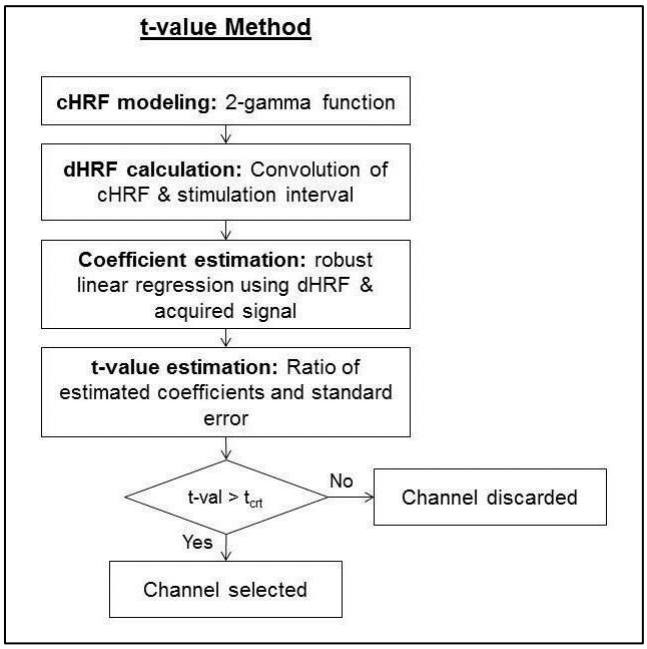

Figure 3.6: Algorithm and stepwise procedure of *t*-value method

Proposed z-score Method

In z-score method, first two steps of modeling cHRF and dHRF is same as *t*-value method. Later, cross correlation technique is implemented between dHRF and acquired pre-processed HbO signal. Correlation is the mutual relationship that exists between two signals and it measures the strength of relationship among one another. Cross correlation, is the type of correlation, which two signals are temporally matched to find out the strength of similarity between each other and mathematical expression is given in equation below:

$$r_{xy}(\tau) = \sum_{-\infty}^{\infty} x(t)y(t-\tau) \tag{3.27}$$

Where τ is the time-lag between x(t) and y(t), the value of r_{xy} denotes the difference (lag/lead) between channel signal y(t) and channel signal x(t). This method has been used earlier for finding relationship of potential dominant channel with its neighboring channels by observing delay in response between the channels [17, 18]. In current study, dHRF signal is swept over measured signal and integral of its product is found at each discrete position 't'. The maximum value of integral product, i.e. correlation coefficient, is selected for each channel showing temporal similarity between two signals at that time instant 'τ'.

$$r^i = \max\left(\sum_{t=-N}^{N} h^i(t)h_M^i(t-\tau)\right) \tag{3.28}$$

The maximum of correlation coefficient 'r' is selected for each channel 'i', between measured hemodynamic response function $h(t)\,\epsilon\, R^{N\,X\,1}$ and dHRF $h_M(t)\epsilon\, R^{N\,X\,1}$, where 'N' is number of samples in the signal. Mean value of measured response is taken for each stimulus type (i.e. LFT, RFT and FT) and afterwards cross correlation is calculated with dHRF. z-scores of correlation coefficients for each channel are then calculated using the formula.

$$z^i = \frac{(r^i - \bar{r})}{\sigma_r} \tag{3.29}$$

Where '$\bar{r}$' is the mean value of correlation coefficients and 'σ_r' is the standard deviation. Only those channels are selected which have positive z-score (i.e. z > 0). The method of channel selection using z-score can be depicted by flow chart as shown in Figure 3.7.

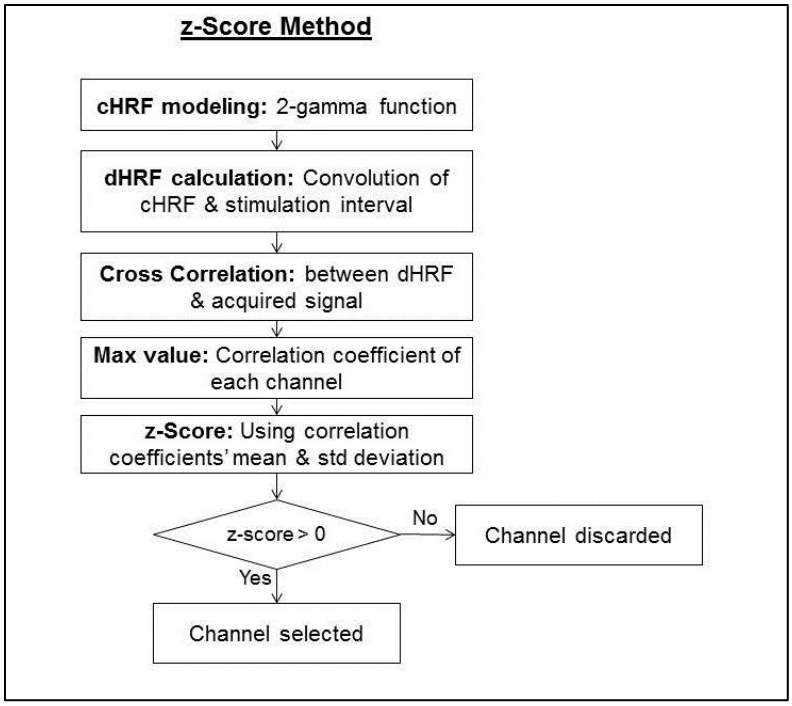

Figure 3.7: Algorithm and stepwise procedure of z-score method

3.2.3 Feature Extraction

After selection of optimal channels through *t*-value and z-score method, the features set of the selected channels and all channels are extracted. The features that have been used in this thesis are mean, peak, slope, skewness, variance and kurtosis of HbO signal. The said features can be easily extracted by calculating statistical parameters of the pre-processed HbO signal. These are also known as conventional BCI features and the most commonly used in fNIRS BCI systems. There have been approaches used with certain window size (0-2s, 2-7s etc) to calculate these features. However, in this study the feature is extracted in entire task window.

As the name describes, **Peak** of the signal is the highest value in the specific time window. It can be find out using *max()* function of MATLAB ®. Mathematically it can be written as follow:

$$Peak = \sum_{t=1}^{N} \max(\Delta C_{HbO}(t)) \tag{3.30}$$

Where, 'N' shows the number of samples and '$\Delta C_{HbO}(t)$' is the input signal. Signal **Mean** is calculated using the following formula:

$$Mean = \mu = \frac{1}{N} \sum_{t=1}^{N} \Delta C_{HbO}(t) \quad (3.31)$$

In order to calculate **Slope** of the signal, there exist two methods. One is to fit a line through data points in specific interval, and second is to find it through start and end points of interval. In this study, line fitting approach was followed by using *polyfit()* function of MATLAB ®. **Variance** is the measurement of scatter present in the data points and it's calculated through following formula:

$$Variance = \sigma^2 = \frac{1}{N-1} \sum_{t=1}^{N-1} (\Delta C_{HbO}(t) - \mu)^2 \quad (3.32)$$

Where 'σ' is the standard deviation and 'μ' is the mean calculated from equation (3.31). **Skewness** of the signal is the measurement of the distortion or asymmetry present around mean value in a normally distributed data. It is measured through following equation:

$$Skewness = E\left[\frac{(\Delta C_{HbO}(t) - \mu)^3}{\sigma^3}\right] \quad (3.33)$$

Where, 'E' is the expected value of '$\Delta C_{HbO}(t)$'. **Kurtosis** differentiates the tail of data curve with normal distribution curve and it's calculated as below:

$$Kurtosis = E\left[\frac{(\Delta C_{HbO}(t) - \mu)^4}{\sigma^4}\right] \quad (3.34)$$

After extraction of above six features, all of them were normalized from a scale of 0 to 1 with the help of following formula:

$$\tilde{X} = \left[\frac{X - \min(X)}{\max(X) - \min(X)}\right] \quad (3.35)$$

Where, '$\tilde{X}$' is the normalized feature vector of original feature vector 'X'.

3.2.4 Classification

The user intentions are identified based on feature sets through regression or classification algorithms. In case of continuously distributed data in the feature space without any distinctive separation, regression algorithms are used to predict the output values. If the

dataset is distributed in feature space with clear decision boundaries then classification techniques are applied on the input labels. The learning algorithms are generally categorized into supervised and unsupervised learning. In supervised learning, a dataset with known input and output labels is used to train and validate a model beforehand and then the output prediction is made on unknown test data. However, in unsupervised learning method, unlabeled dataset is provided to the model and it tries to group the similar dataset into clusters and subsequently these clusters are used as classes for further classification of data.

The implementation of supervised classification algorithms in BCI system are known to be the most popular. In this current study, Linear Discriminant Analysis (LDA) method is applied for classification of two-class problem (Activity vs Rest). LDA is one of the most commonly used classifier in fNIRS-BCI [6], [7] due to its simplicity, acceptable classification accuracy and lower computational requirements. Nonetheless, its classification accuracy is sometimes compromised due to presence of strong noise or outliers in the data. LDA tends to draw a linear feature subspace to discriminate between two or more classes of multiple features. It is basically transformation technique used for dimensionality reduction algorithm but it's also a robust classifier. The selection of decision boundary or hyperplane, on which data is projected, is based on the criteria that results in maximum distance of intra-class means and minimum value of inter-class variance. The aforementioned criteria is also known as Fisher's criteria and purpose of it is to maximizes the following objective function:

$$J(W) = \frac{|W^T S_B W|}{|W^T S_W W|} \tag{3.36}$$

Where, W is the projection matrix onto which data is projected, S_W is the within the class scatter matrix and S_B is the between class scatter matrix. Both of these matrices are formulated as below:

$$S_B = \sum_{c=1}^{n} k_c(\mu_c - \bar{x})(\mu_c - \bar{x})^T \tag{3.37}$$

$$S_W = \sum_{c=1}^{n} \sum_{x_i \in Class\ c} (x_i - \mu_c)(x_i - \mu_c)^T \tag{3.38}$$

'μ_c' is the mean within the class while '$\bar{x}$' is the overall mean of the dataset, 'n' denotes the number of classes, 'k_c' is number of samples in class 'c'. If we can reformulate the equation (3.28), it can look like a generalized eigenvector problem:

$$S_W{}^{-1} S_B W = \lambda W \tag{3.39}$$

From above equation, we can obtain the optimal projection matrix 'W' by finding the corresponding largest eigenvalue 'λ'. Finally, the original data 'X' is projected onto new feature space 'X'' by projection matrix 'W'.

$$X' = XW \tag{3.40}$$

The set of classes in newly transformed data are then discriminated and classification accuracy is obtained. The dataset was validated and tested through leave-one-out-cross-validation (LOOCV) technique. Through MATLAB ® commands *cvpartition(), classify() & crossval ()* the dataset was partitioned into folds, classified and cross validated, respectively.

CHAPTER 4: RESULTS AND DISCUSSION

4.1 Results

The result obtained from the proposed method and conventional *t*-value method show that there is difference in selected channels for specific task type. It can also be seen in the activation maps that the three specified activities (i.e. RFT vs Rest, LFT vs Rest and FT vs Rest) are showing deviation in cortical activations for both the applied methods. The activation maps for subject 9 and subject 13 can be depicted in Figure 4.1 and Figure 4.2, respectively. It can be clearly seen that variations in activations have been occurred for both subjects. These differences are due to existence of anatomical and physical variations between each subject. Moreover, activation maps also portray that different brain regions are energized for different tasks and different subjects.

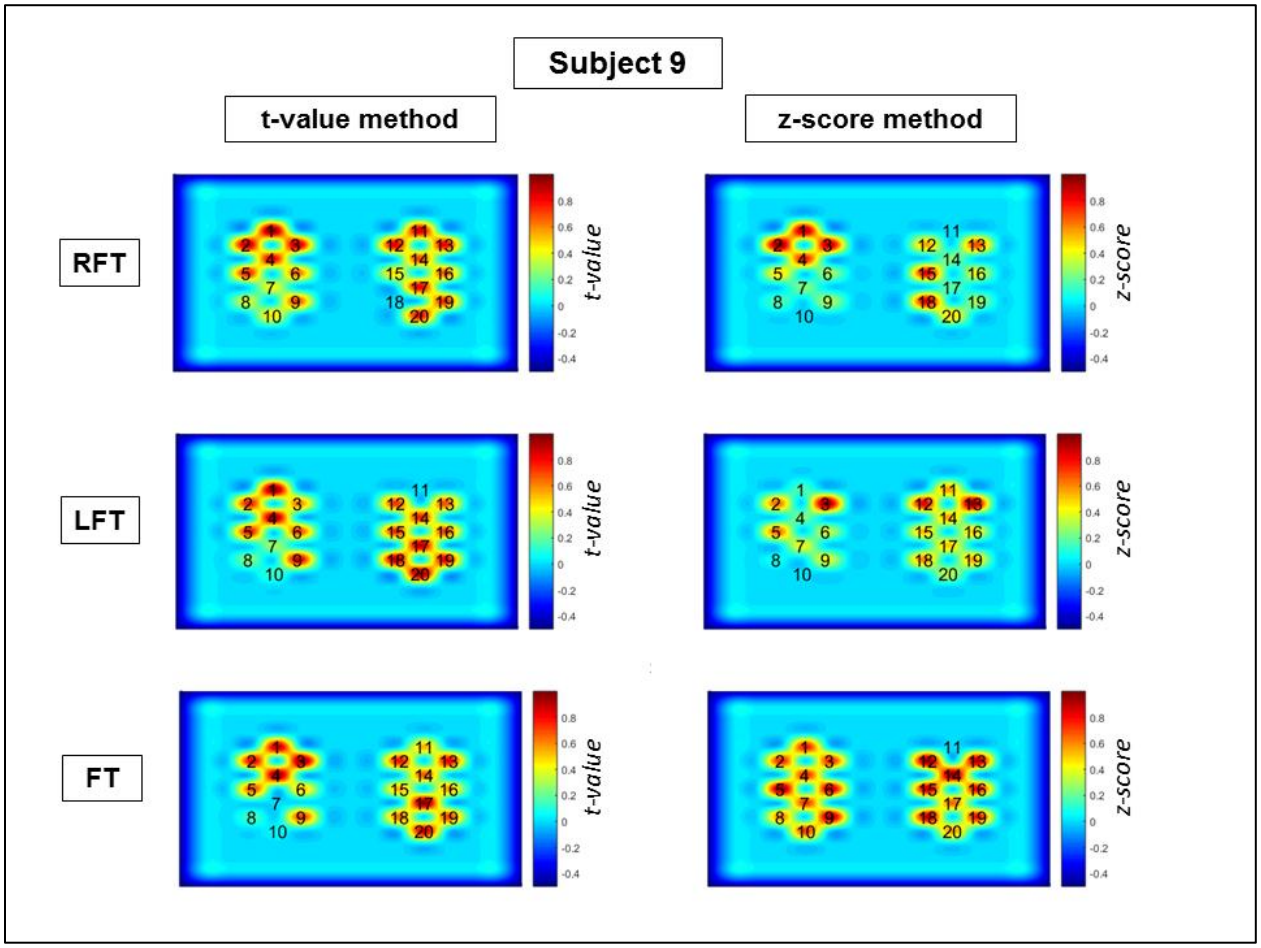

Figure 4.1: Activation map of subject 9 for RFT, LFT and FT tasks obtained by *t*-value and z-score methods

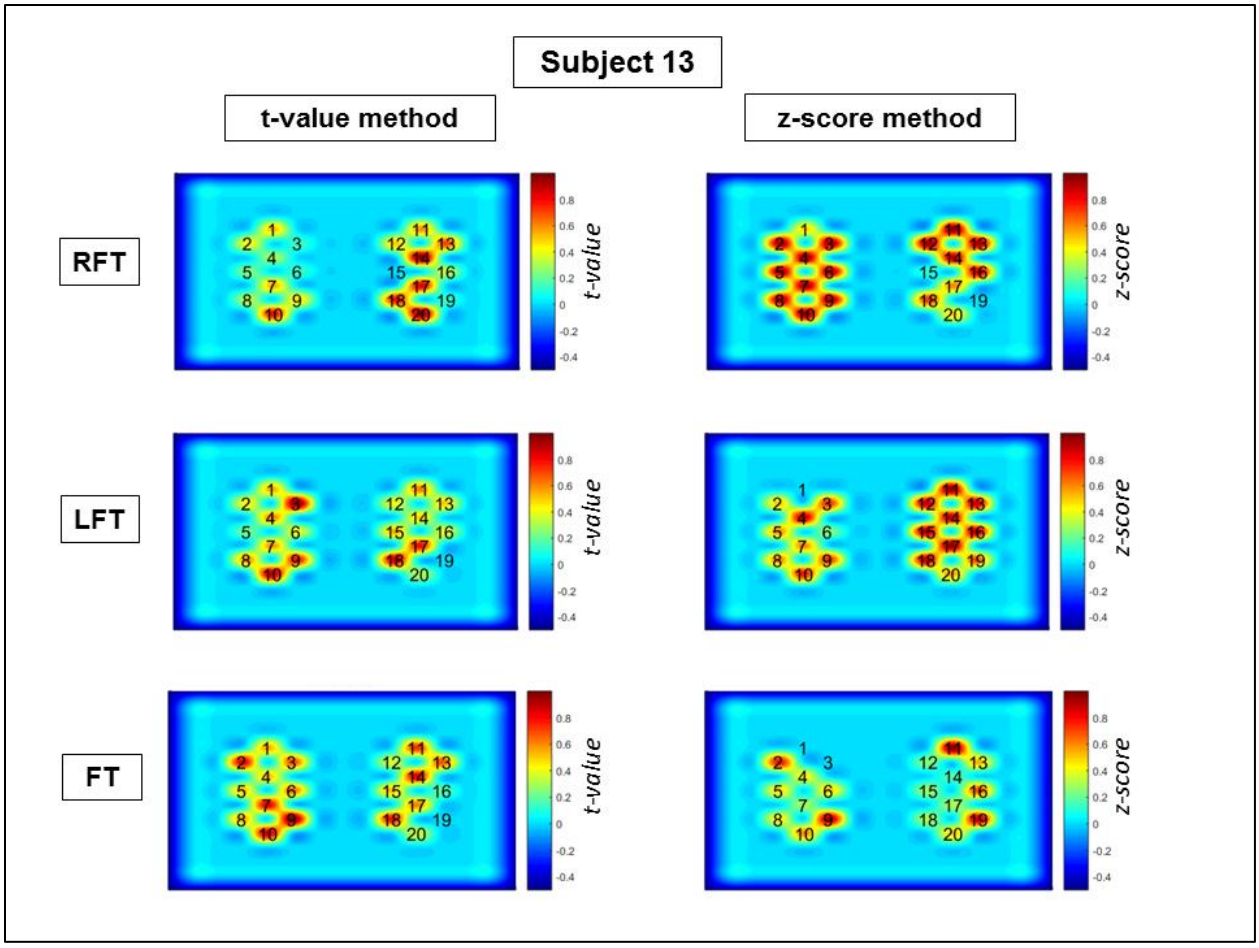

Figure 4.2: Activation map of subject 13 for RFT, LFT and FT tasks obtained by *t*-value and z-score methods

The number of channels selected for RFT task by z-score and *t*-value method is given in Table 4.1. The total number of selected channels using *t*-value method range from 2-20 and for z-score method the chosen channels varies between 10-16. The total number of common channels range from 1-15. Similarly, details of dominant channels for LFT task using *t*-value and proposed z-score methods are represented in Table 4.2. The range of selected number channels for aforementioned task for *t*-value and z-score methods are 8-20 and 9-16, respectively. The common number of channels for LFT task varies from 4-14. Likewise, subject-wise details of selected channels for FT task is being displayed in Table 4.3. The selected channels for FT task through *t*-value and z-score method range from 6-20 and 8-17 respectively. The common number of active channels for both the methods are from 2-16 for the said task. It is also clear from the results explained earlier that the selected active channels have distinction w.r.t subject, tasks and

methods applied. However, despite the differences yet there exist common active channels between both the techniques.

Table 4.1: Comparative details of channels selected through *t*-value and z-score methods for RFT vs Rest task

	Right Hand Finger Tapping (RFT)				
	t-value method		z-score method		Total number of common channels
	Selected Channels	Total number of channels	Selected Channels	Total number of channels	
Sub1	3-6	4	1-7,10-14,16	13	4
Sub2	2,11	2	1-10,12-13,18,20	14	1
Sub3	1-20	20	2,4-5,7-8,13-16,18,20	11	11
Sub4	1,5,7-8,11-15,18-20	12	3-9,11-15,17-20	16	11
Sub5	1-20	20	4-10,14-20	14	14
Sub6	1-20	20	1-4,7-10,12-14,17-20	15	15
Sub7	2,4-11, 14,18-20	13	3-8,11,14,19-20	10	9
Sub8	1-20	20	1-5,7-9,11,14,16,18-20	14	14
Sub9	1-4,11-13,17,20	9	1-4,7-8,11-15,18,19	13	7
Sub10	2-7,9-15,17-20	17	2,4-9,11-19	16	14
Sub11	2,8-10, 12,15,17-20	10	1-3,5-11,14-15,17-20	16	9
Sub12	2-10,14-15,17-20	15	1-13,18-20	16	12
Sub13	1-2,7-20	16	2-14,16	14	10
Sub14	1-20	20	2-5,7-11,14-15,18-20	14	14
Sub15	2-13,15-20	18	2-12,15,18-19	14	14
Sub16	1,3-5,7,11-20	15	2,4-11,15,18-20	13	8
Sub17	1-7,9,12-14,17-20	15	2-7,9,11-12,17-20	13	12

Table 4.2: Comparative details of channels selected through *t*-value and z-score methods for LFT vs Rest task

	Left Hand Finger Tapping (LFT)				
	t-value method		z-score method		Total number of common channels
	Selected Channels	Total number of channels	Selected Channels	Total number of channels	
Sub1	2-3,11-20	12	3,5-6,8,10,12-16	10	6
Sub2	4-10,13-20	15	5,7,11,13-14,17-20	9	8
Sub3	1-20	20	1,6-9,11,17-18,20	9	9
Sub4	1,4,8,10-20	14	2-4,7-10,12-20	16	12
Sub5	1-20	20	2-3,5-6,8,10,12,14-20	14	14
Sub6	1-20	20	1-3,5-10,16,18-20	13	13
Sub7	1-20	20	3-5,7,10-16,18-20	14	14
Sub8	1-20	20	2-4,7-8,10,13-14,16-20	13	13
Sub9	1-2,4-5,9,14-15,17-20	11	1-3,5,7,10,12-13,16,18	10	4
Sub10	1-6,10-18,20	16	2-6,9-19	16	14
Sub11	2,6-10,13,17-20	11	6-10,12-15,17-20	13	10
Sub12	3,7-11,15,20	8	1-3,8-9,12-16,18-20	13	5
Sub13	1-4,6-11,15,17-18	13	3-4,7-18	14	10
Sub14	1-20	20	2-6,9-11,14-17,19-20	14	14
Sub15	4-10,14-20	14	1-5,9-14,17-20	15	9
Sub16	1-3,5,7-8,11-16	12	1-3,5,7,9,11-13,15-18, 20	14	10
Sub17	1-3,11-16,20	10	1,5-8,10,12,14-17,19-20	13	6

Table 4.3: Comparative details of channels selected through *t*-value and z-score methods for FT vs Rest task

	Foot Tapping (FT)				
	t-value method		z-score method		Total number of common channels
	Selected Channels	Total number of channels	Selected Channels	Total number of channels	
Sub1	1,3,11,14,19-20	6	2,4-9,11-13,16,20	12	2
Sub2	2-5,7-11,13,17-18,20	13	1-3,8-11,13	8	7
Sub3	1-20	20	1-5,7-11,13-14,16,18-20	16	16
Sub4	1,3,7-15,17-20	15	1,3,7-10,12-13,16-20	13	12
Sub5	1-20	20	5-6,8-9,11-20	14	14
Sub6	1-20	20	4,6-7,9,11-18,20	13	13
Sub7	1-20	20	3,6-15,17-20	15	15
Sub8	1-20	20	1-2,6,10-15,17-18,20	12	12
Sub9	1-5,9,11-14,17-20	14	1-6,9,12-15,17-20	15	13
Sub10	1-4,6,8,11-13	9	1-2,4-5,7,9,11-16,19-20	14	6
Sub11	3-20	18	1-10,12-13,16-20	17	15
Sub12	1-20	20	2,4-13,16-20	16	16
Sub13	2-3,6-11,13-14,17-18	12	2,5-7,9-13,16,19	11	7
Sub14	1-20	20	1-8,10-14,16,18	15	15
Sub15	1-10,13-20	18	2-3,5,7,11-20	14	12
Sub16	4-9,11-20	16	2,5,7,9-16,18	12	10
Sub17	1-3,6-10,12,14-15, 17-20	15	1-3,5-10,13-14,16-18,20	15	12

Post selection of active channels, statistical spatio-temporal features i.e. mean, peak, slope, variance, skewness and kurtosis are extracted from the chosen channels. Additionally, the stated features for all channels were also extracted in order to obtain classification accuracy for further validation of proposed methodology. 3-dimensional feature scatter plots of mean, peak and slope and 2-dimensional feature scatter plot of mean and peak for *t*-value selected channels, z-score selected channels and all channels i.e. without any selection have been plotted for each task. The said for subject 9 are shown in Figures 4.3, 4.4 and 4.5 respectively; while the feature scatter plots for RFT, LFT and FT tasks for subject 13 are correspondingly shown in Figures 4.6, 4.7 and 4.8.

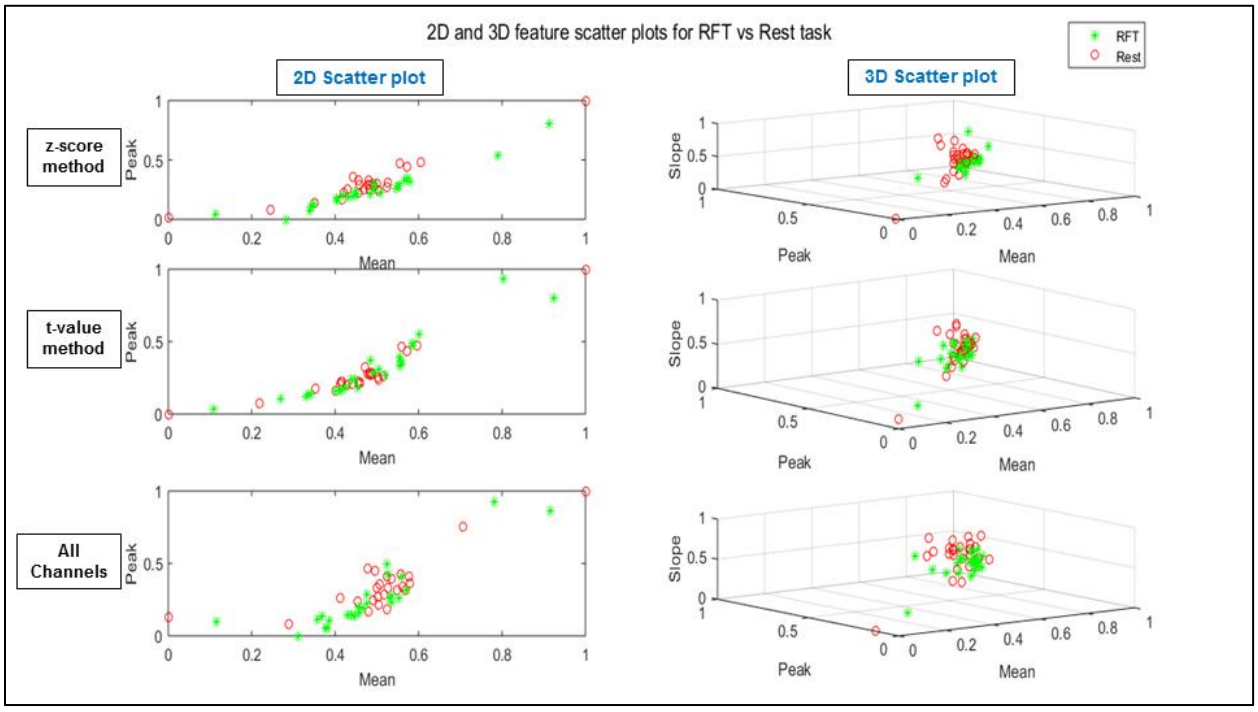

Figure 4.3: Feature scatter plot of RFT vs Rest task for channels selected by using *t*-value method, z-score method and all channels for subject 9

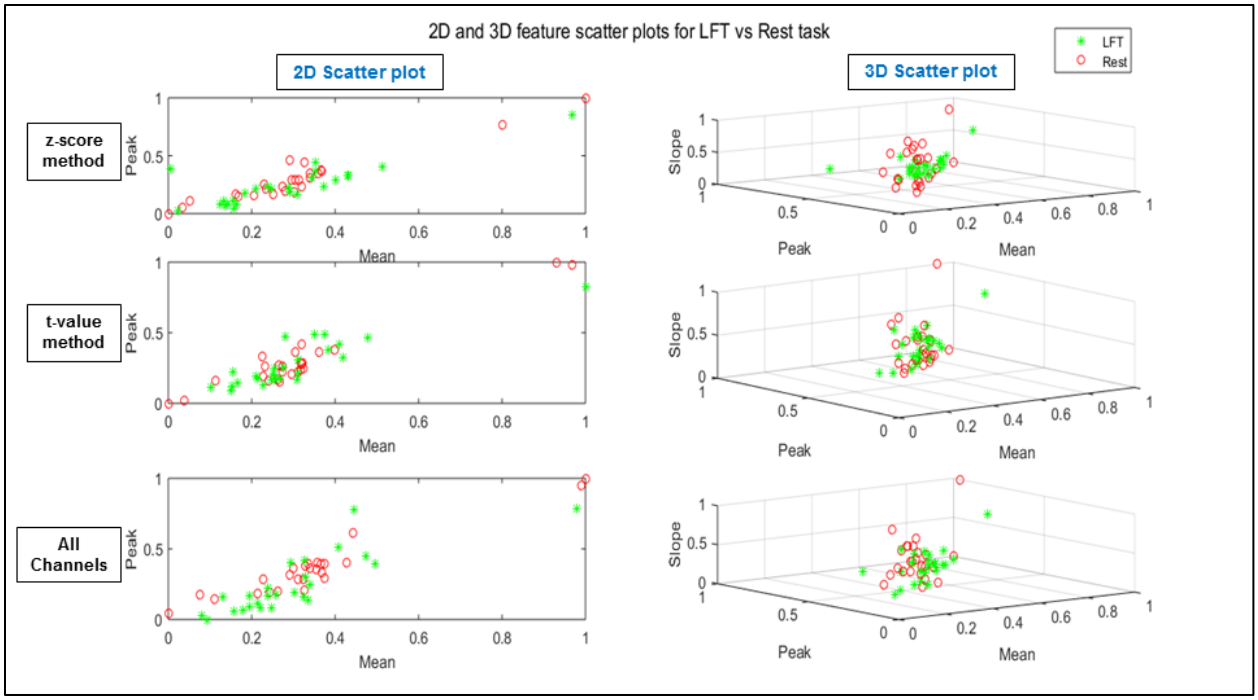

Figure 4.4: Feature scatter plot of LFT vs Rest task for channels selected by using *t*-value method, z-score method and all channels for subject 9

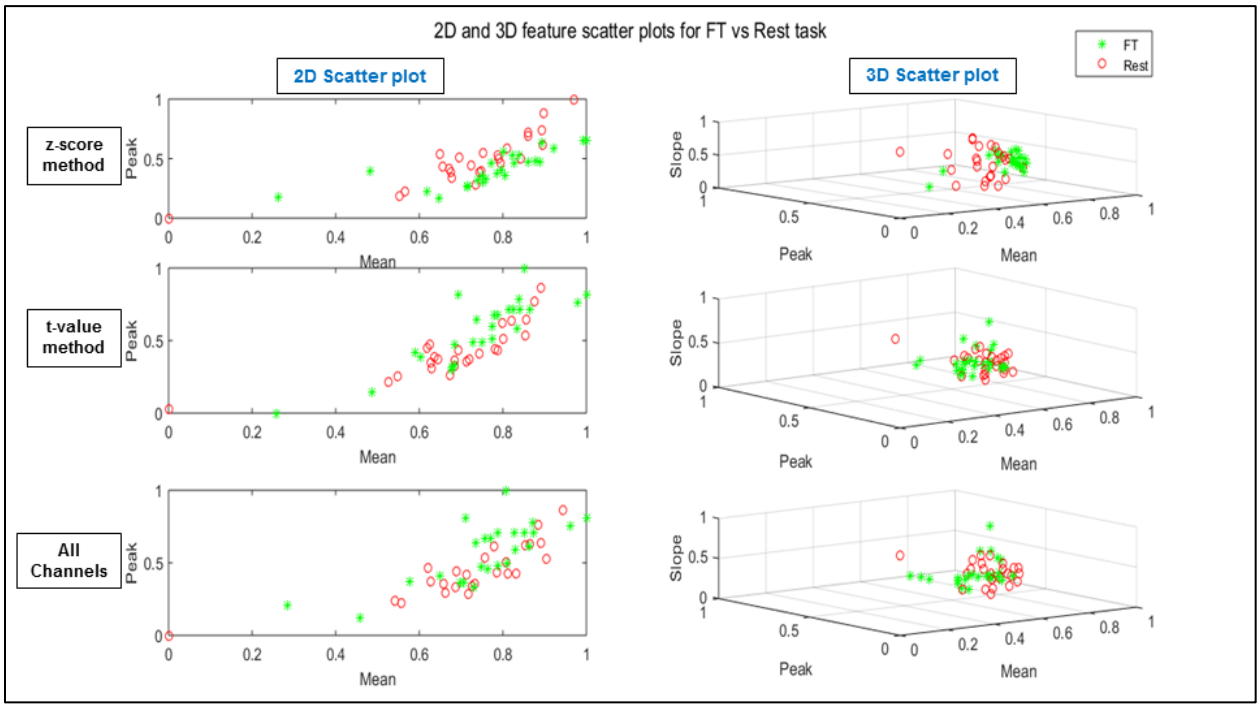

Figure 4.5: Feature scatter plot of FT vs Rest task for channels selected by using *t*-value method, z-score method and all channels for subject 9

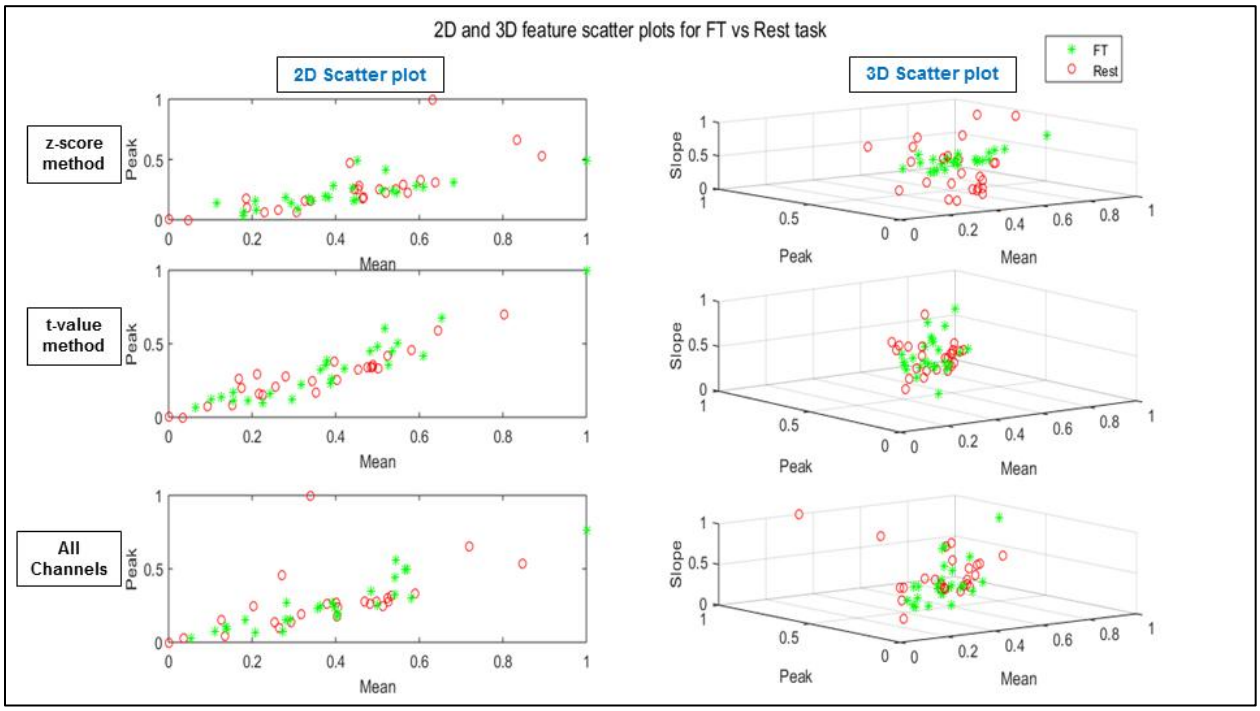

Figure 4.6: Feature scatter plot of RFT vs Rest task for channels selected by using *t*-value method, z-score method and all channels for subject 13

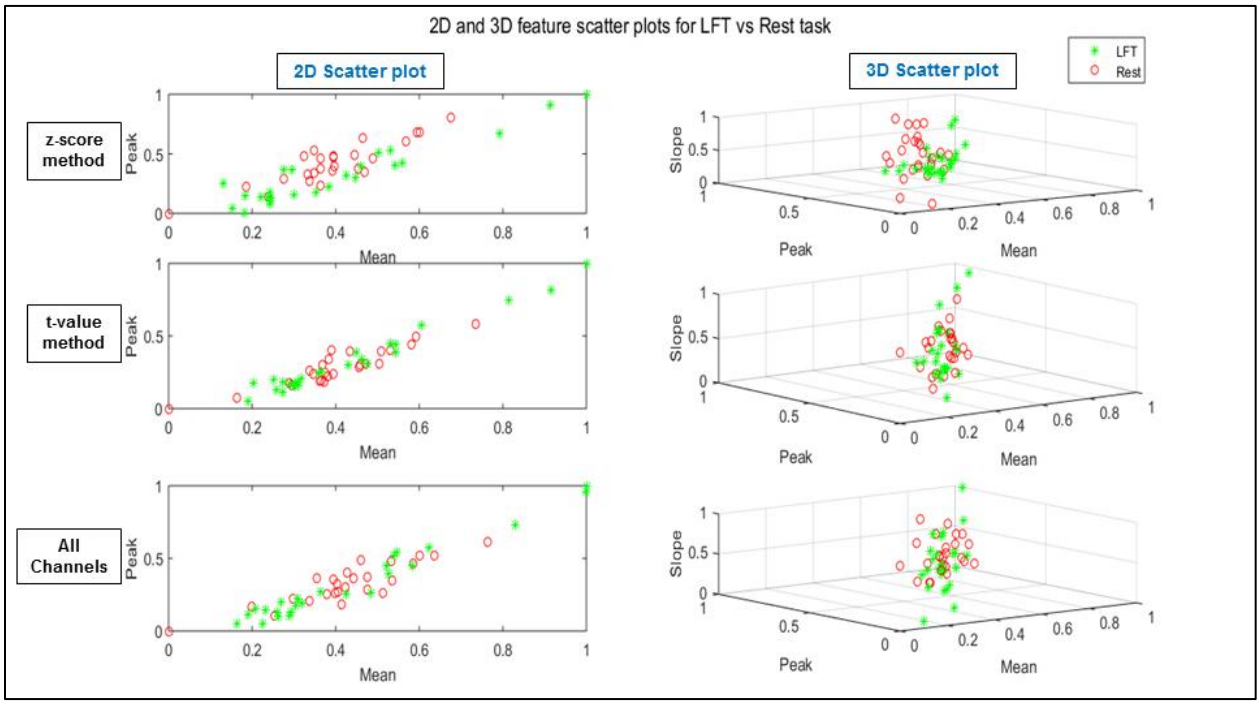

Figure 4.7: Feature scatter plot of LFT vs Rest task for channels selected by using *t*-value method, z-score method and all channels for subject 13

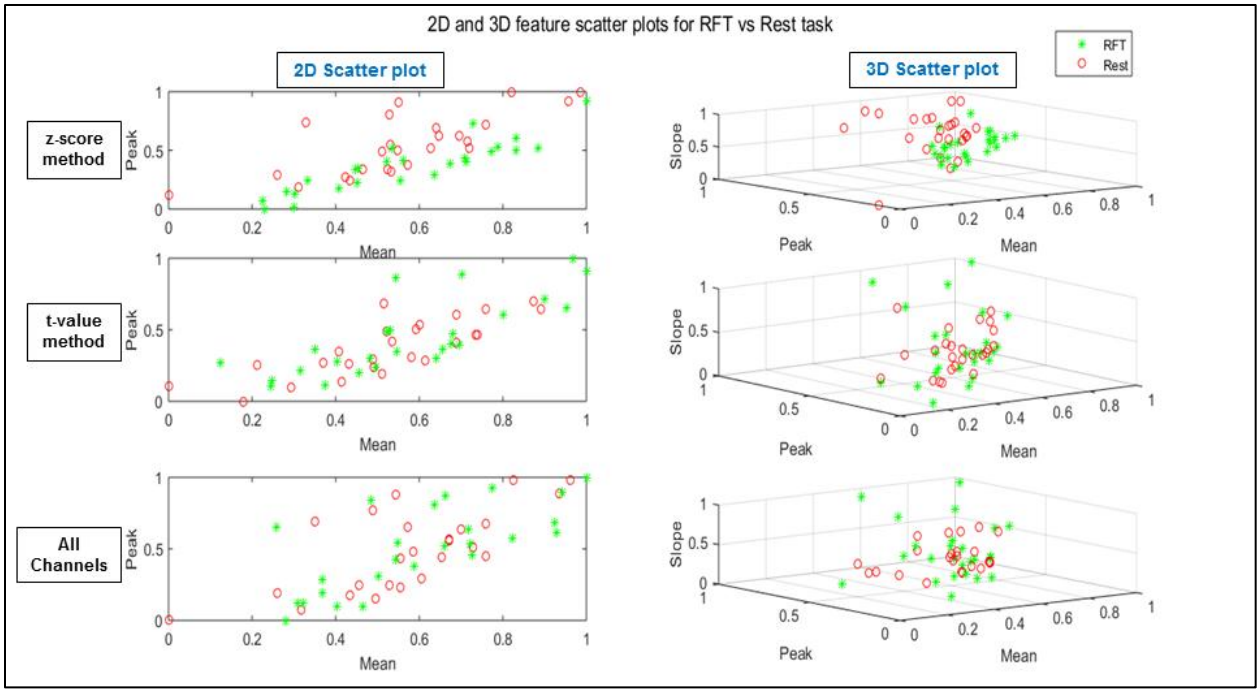

Figure 4.8: Feature scatter plot of FT vs Rest task for channels selected by using *t*-value method, z-score method and all channels for subject 13

The classification accuracies of across all 17 subjects achieved using LDA with 2-class (Task vs Rest) problem for RFT, LFT and FT tasks are tabulated in Tables 4.4, 4.5 and 4.6 respectively. The tables display comparative analysis of classification accuracies of nominated channels obtained from z-score based method, *t*-value method and using all channels on all three tasks. The mean accuracies of all subjects and standard deviations are also displayed in the tables as well as in the bar chart graph, as depicted in Figure 4.9. It is evident from the results that improved classification accuracies have been resulted from proposed z-score method in all three tasks with average accuracies of **72.24 ± 6.2%**, **72 ± 8.1%** and **69.41 ± 6.7%** for RFT, LFT and FT tasks respectively. However, the results obtained from *t*-value method for RFT, LFT and FT tasks are **51.29 ± 13.1%**, **51.53 ± 12%** and **54.12 ± 10.1%** respectively. Nevertheless, accuracies obtained by selecting all channels resulted in classification accuracies of **54.71 ± 10.3%**, **54.47 ± 14.2%** and **54.12 ± 11.1%** for RFT, LFT and FT tasks respectively. It can be also seen from the results that *t*-value method accuracies for RFT and LFT tasks were lower as compared to all channel accuracies. The statistical verification of the results obtained by z-score method in comparison to *t*-value method and all channel data results were carried out by applying two-tailed paired sample Student's *t*-test. For comparison of two hypothesis, Bonferroni correction is

being used to find the adjusted confidence interval level of 0.0167. Table 4.7 shows the *p*-values obtained for two comparisons for each task: z-score method vs *t*-value method and z-score method vs all channels. It can be seen from the results that performance of the proposed z-score method selected channels are significantly better ($p<0.0167$) than conventional *t*-value method selected channels and by using all channels for RFT vs rest, LFT vs rest and FT vs rest tasks.

Table 4.4: Comparison of Classification accuracies obtained through z-score method, *t*-value method and all channels for RFT vs Rest task.

	RIGHT HAND FINGER TAPPING (RFT)		
	z-score	***t*-value**	**All channels**
Sub 1	62	52	46
Sub 2	64	38	44
Sub 3	82	64	64
Sub 4	78	36	42
Sub 5	74	64	64
Sub 6	70	68	68
Sub 7	76	50	54
Sub 8	70	50	50
Sub 9	76	50	66
Sub 10	60	68	64
Sub 11	70	22	56
Sub 12	66	50	40
Sub 13	74	40	46
Sub 14	78	70	70
Sub 15	74	42	40
Sub 16	76	52	58
Sub 17	78	56	58
Mean	**72.24%**	**51.29%**	**54.71%**
Std. Dev	**6.2**	**13.1**	**10.3**

Table 4.5: Comparison of Classification accuracies obtained through z-score method, *t*-value method and all channels for LFT vs Rest task.

	LEFT HAND FINGER TAPPING (LFT)		
	z-score	***t*-value**	**All channels**
Sub 1	68	50	62
Sub 2	60	40	48
Sub 3	72	72	72
Sub 4	64	56	58
Sub 5	76	58	58
Sub 6	84	66	66
Sub 7	68	62	62
Sub 8	66	52	52
Sub 9	84	50	66
Sub 10	68	62	70
Sub 11	64	28	20
Sub 12	78	56	56
Sub 13	86	40	62
Sub 14	70	62	62
Sub 15	78	48	40
Sub 16	76	40	40
Sub 17	62	34	32
Mean	**72%**	**51.53%**	**54.47%**
Std. Dev	**8.1**	**12**	**14.2**

Table 4.6: Comparison of Classification accuracies obtained through z-score method, *t*-value method and all channels for FT vs Rest task.

	FOOT TAPPING (FT)		
	z-score	***t*-value**	**All channels**
Sub 1	68	34	24
Sub 2	60	54	54
Sub 3	80	66	66
Sub 4	62	44	48
Sub 5	60	48	48
Sub 6	70	66	66
Sub 7	76	72	72
Sub 8	78	64	64
Sub 9	70	54	56
Sub 10	60	52	48
Sub 11	68	54	46
Sub 12	64	48	48
Sub 13	68	46	58
Sub 14	72	62	62
Sub 15	72	52	50
Sub 16	72	42	50
Sub 17	80	62	60
Mean	**69.41%**	**54.12%**	**54.12%**
Std. Dev	**6.7**	**10.1**	**11.1**

Table 4.7: Statistical significance of the proposed z-score method

	Bonferroni correction applied ($p < 0.0167$)		
	RFT vs rest	**LFT vs rest**	**FT vs rest**
z-score method vs *t*-value method	1.24E-06	1.82E-06	1.08E-05
z-score method vs all channels	1.10E-06	1.05E-04	2.95E-05

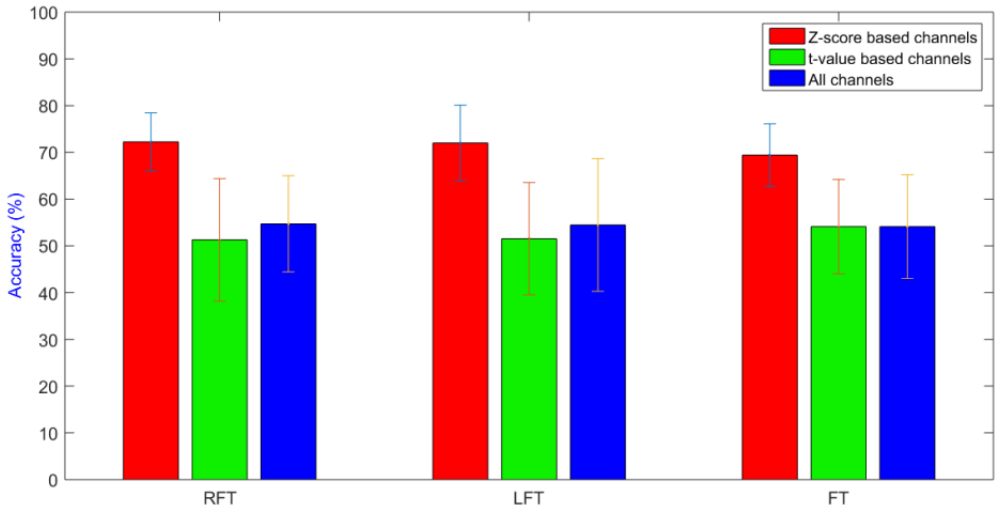

Figure 4.9: Average classification accuracies of RFT, LFT and FT tasks obtained with z-score selected channels, *t*-value selected channels and all channels.

4.2 Discussion

This research focuses on enhancement of classification accuracy by choosing optimal channels with the help of newly proposed approach. Previously studies have been conducted for improvement in classification accuracies through implementation of algorithms at different stages of BCI. Some researchers have used different temporal information of task data [18], [21], [35]–[37] to increase fNIRS-BCI performance. Optimal feature combinations [18], [38] have also been tried for improvement in the performance. Similarly, extraction and selection of optimal features [39]–[41] have been implemented as well to increase the desired classification accuracy. Additionally, different classifiers [18], [42]–[45] have also been used for optimization of classification results. Moreover, different channel selection algorithms have also been proposed previously for performance improvement of fNIRS-BCI systems which includes *t*-value method [16], [17], [20], [46], baseline correction method [21], cross correlation method [22], [23] and others [16], [24]–[28].

Out of the aforementioned channel selection methods, the *t*-value method is a conventionally applied technique firstly used by Santosa et al. (2014) [19] in which determination of active stimulus of auditory response was carried out. Later, it was applied by

Hong & Santosa (2016) [20], Nguyen & Hong (2016) [16] and Nguyen et. al (2016) [17] in their studies for selecting active channels. The cross correlation method for selection of cortically active channels, as applied by Rojas et al. (2016) [22], [23], have been applied to find a relationship between potential dominant channels and the neighboring channels in both hemisphere by calculating lag between each other.

In this thesis cross correlation method has also been implemented but the proposed methodology is novel as compared to previously conducted method because of two reasons. a) This study covers the scope of BCI which was not covered before. b) This study applied cross correlation between desired hemodynamic response function (dHRF) and acquired cortical signal. Afterwards, the maximum of correlation values are segregated against each channel and z-score is applied on these maximum correlation coefficients. Later, z-score is used to find out the active channels based on positive value of z-score of each channel.

Additionally, this study is also unique in a sense that it comparatively analyses proposed channel selection method with already existing *t*-value method. However, previously *t*-value method has been applied independently for identification of dominant channels without drawing any comparison. Moreover, further validation of proposed method was performed by calculating classification accuracy on all channels i.e. without any channel selection method. Another validation of proposed z-score method is based on using three different brain activation tasks. The results have shown that the proposed method performed better, in terms of classification accuracy, than *t*-value method and all selected channels for three tasks based fNIRS-BCI. Improvements in classification accuracies from 51.29±13.1% to 72.24±6.2% for RFT vs rest, from 51.53±12% to 72±8.1% for LFT vs rest, and from 54.12±11.1% to 69.41±6.7% for FT vs rest tasks were observed. The selected channels results also portrays that active channels in each subject with one another were inconsistent and it also non-uniformly differs with each activity. This suggests the existence of variation between each subject w.r.t brain size and anatomical variations. Due to these reasons, it is extremely important for obtaining superior performance that correct channel and region of interest in identified.

The technical evaluation of improvement in performance due to the proposed method suggests that it might be due to the reason that activity in brain is more significantly and informatively translated as compared to *t*-value method. The *t*-value method corresponds to linear regression of the mathematical model with actual and desired signal and later finding out the statistical significance of the estimated coefficients. The actual response and the desired response are used to estimate parameters that best fit the original response. The statistical significance of the estimated coefficients are calculated by calculating ratio of the weighted coefficients with its standard error. Positive *t*-value ($t>0$) or greater than threshold value ($t>t_{crt}$) suggests that whether the channels is active or not. However, the proposed method uses temporal information of the cortical activity and correlates the actual and desired signal. The degree of similarity and strength is measured in case of z-score method and it quantifies how much the actual signal and desired signal relate to one another. The more associated the actual signal is to the desired signal w.r.t its temporal features the more active the channel will be. Thereby, the maximum of correlation coefficient between the signals suggest the maximum strength of similarity between one another. Besides, the z-score which measures the distance of point from the mean of data and positive z-score quantifies that signal is cortically active or otherwise. Hence, cortical activity based channel selection possesses more useful and inherent brain information which plays useful part into enhancing performance of fNIRS-BCI system.

CHAPTER 5: CONCLUSION AND RECOMMENDATIONS

The current study targeted the selection of optimal number of channels for fNIRS-BCI system with the main purpose of improvement in classification accuracy. In order to achieve the performance improvement, a novel method have been proposed in which first cross correlation is used between desired hemodynamic response function and acquired cortical signal. The results of maximum correlation coefficients are gathered from each channel and later z-scores are calculated on the resulted maximum coefficients. The positive z-score value ($z > 0$) signifies the active channel of interest (COI). Already existing *t*-value method for channel selection has also been used to validate the results of the proposed z-score method and the results were also compared without using channel selection algorithms i.e. using all the channels. The spatio-temporal features i.e. mean, peak, slope, skewness, kurtosis and variance of HbO signal were used on LDA classifier. The results achieved through proposed method on a 2-class problem for RFT vs rest, LFT vs rest and FT vs rest showed improvement in classification accuracies from 51.29±13.1% to 72.24±6.2%, 51.53±12% to 72±8.1%, 54.12±11.1% to 69.41±6.7% respectively. The results showed that proposed method is a progression in already existing channel selection techniques and can identify channels of interest based on active cortical region more effectively through enhancement in classification accuracies of fNIRS-BCI.

Nevertheless, despite showing increased classification performance yet the proposed method poses few limitations. Firstly, this method can be applied to a single task at a time as a particular brain region is associated with a specific activity. Secondly, specific channels remained active for specific subject due to the reason that variations exist in brain sizes across multiple subjects. Moreover, LDA based classification model was applied in the current thesis mainly because of its simplicity, speedy performance and it is computationally less expensive. Due to the above mentioned reasons, LDA is commonly used for the fNIRS-BCI systems [6], [42]. In order to further improve classification performance, other state-of-the-art classifiers like CNN, DNN, Ensemble classifiers or other deep learning algorithms may also be applied for analysis [7]. Additionally, optimal features combinations and vector phase analysis based features [38]–[41] can also be applied to enhance classification accuracies.

REFERENCES

[1] J. Wolpaw, N. Birbaumer, D. Mcfarland, G. Pfurtscheller, and T. Vaughan, "Wolpaw, J.R.: Brain-computer interfaces for communication and control. 'Clin. Neurophysio1. 113, 767-791," *Clin. Neurophysiol.*, vol. 113, pp. 767–791, Jul. 2002, doi: 10.1016/S1388-2457(02)00057-3.

[2] U. Chaudhary, N. Birbaumer, and A. Ramos-Murguialday, "Brain-computer interfaces for communication and rehabilitation," *Nat. Rev. Neurol.*, vol. 12, no. 9, pp. 513–525, 2016, doi: 10.1038/nrneurol.2016.113.

[3] M. A. Lebedev and M. A. L. Nicolelis, "Brain-machine interfaces: past, present and future," *Trends Neurosci.*, vol. 29, no. 9, pp. 536–546, Sep. 2006, doi: 10.1016/j.tins.2006.07.004.

[4] P. Konrad and T. Shanks, "Implantable brain computer interface: Challenges to neurotechnology translation," *Neurobiol. Dis.*, vol. 38, pp. 369–375, Jun. 2010, doi: 10.1016/j.nbd.2009.12.007.

[5] T. O. Zander, C. Kothe, S. Jatzev, and M. Gaertner, "Enhancing Human-Computer Interaction with Input from Active and Passive Brain-Computer Interfaces," pp. 181–199, 2010, doi: 10.1007/978-1-84996-272-8_11.

[6] N. Naseer and K. S. Hong, "fNIRS-based brain-computer interfaces: A review," *Front. Hum. Neurosci.*, vol. 9, no. JAN, pp. 1–15, 2015, doi: 10.3389/fnhum.2015.00003.

[7] K. S. Hong, M. J. Khan, and M. J. Hong, "Feature Extraction and Classification Methods for Hybrid fNIRS-EEG Brain-Computer Interfaces," *Front. Hum. Neurosci.*, vol. 12, no. June, pp. 1–25, 2018, doi: 10.3389/fnhum.2018.00246.

[8] F. F. Jobsis, "Noninvasive, infrared monitoring of cerebral and myocardial oxygen sufficiency and circulatory parameters," *Science (80-.).*, vol. 198, no. 4323, pp. 1264 LP – 1267, Dec. 1977, doi: 10.1126/science.929199.

[9] S. Coyle, T. Ward, C. Markham, and G. Mcdarby, "On the suitability of near-infrared (NIR) systems for next-generation brain-computer interfaces," *Physiol. Meas.*, vol. 25, pp. 815–822, Sep. 2004, doi: 10.1088/0967-3334/25/4/003.

[10] D. T. Delpy, M. Cope, P. Van Der Zee, S. Arridge, S. Wray, and J. Wyatt, "Estimation of optical pathlength through tissue from direct time of flight measurement," *Phys. Med. Biol.*, vol. 33, no. 12, pp. 1433–1442, 1988, doi: 10.1088/0031-9155/33/12/008.

[11] G. Gratton, C. R. Brumback, B. A. Gordon, M. A. Pearson, K. A. Low, and M. Fabiani, "Effects of measurement method, wavelength, and source-detector distance on the fast optical signal.," *Neuroimage*, vol. 32, no. 4, pp. 1576–1590, Oct. 2006, doi: 10.1016/j.neuroimage.2006.05.030.

[12] L. Gagnon *et al.*, "Quantification of the cortical contribution to the NIRS signal over the motor cortex using concurrent NIRS-fMRI measurements," *Neuroimage*, vol. 59, no. 4, pp. 3933–3940, 2012, doi: https://doi.org/10.1016/j.neuroimage.2011.10.054.

[13] R. A. Poldrack, "Region of interest analysis for fMRI.," *Soc. Cogn. Affect. Neurosci.*, vol. 2, no. 1, pp. 67–70, Mar. 2007, doi: 10.1093/scan/nsm006.

[14] V. Jurcak, D. Tsuzuki, and I. Dan, "10/20, 10/10, and 10/5 systems revisited: their validity as relative head-surface-based positioning systems.," *Neuroimage*, vol. 34, no. 4, pp. 1600–1611, Feb. 2007, doi: 10.1016/j.neuroimage.2006.09.024.

[15] G. A. Zimeo Morais, J. B. Balardin, and J. R. Sato, "fNIRS Optodes' Location Decider (fOLD): a toolbox for probe arrangement guided by brain regions-of-interest," *Sci. Rep.*, vol. 8, no. 1, p. 3341, 2018, doi: 10.1038/s41598-018-21716-z.

[16] H.-D. Nguyen and K.-S. Hong, "Bundled-optode implementation for 3D imaging in functional near-infrared spectroscopy," *Biomed. Opt. Express*, vol. 7, no. 9, p. 3491, 2016, doi: 10.1364/boe.7.003491.

[17] H. D. Nguyen, K. S. Hong, and Y. Il Shin, "Bundled-optode method in functional near-infrared spectroscopy," *PLoS One*, vol. 11, no. 10, pp. 1–23, 2016, doi: 10.1371/journal.pone.0165146.

[18] M. J. Khan and K.-S. Hong, "Passive BCI based on drowsiness detection: an fNIRS study," *Biomed. Opt. Express*, vol. 6, no. 10, p. 4063, 2015, doi: 10.1364/boe.6.004063.

[19] H. Santosa, M. J. Hong, and K. S. Hong, "Lateralization of music processing with noises in the auditory cortex: An fNIRS study," *Front. Behav. Neurosci.*, vol. 8, no. DEC, pp. 1–9, 2014, doi: 10.3389/fnbeh.2014.00418.

[20] K. S. Hong and H. Santosa, "Decoding four different sound-categories in the auditory cortex using functional near-infrared spectroscopy," *Hear. Res.*, vol. 333, pp. 157–166, 2016, doi: 10.1016/j.heares.2016.01.009.

[21] M. J. Khan and K. S. Hong, "Hybrid EEG-FNIRS-based eight-command decoding for BCI: Application to quadcopter control," *Front. Neurorobot.*, vol. 11, no. FEB, 2017, doi: 10.3389/fnbot.2017.00006.

[22] R. F. Rojas, X. Huang, and J. L. Aparicio, "NIRS-Based Cortical Activation Analysis by Temporal Cross Correlation," *Signal Image Process. An Int. J.*, vol. 7, no. 1, pp. 31–41, 2016, doi: 10.5121/sipij.2016.7104.

[23] R. F. Rojas, X. Huanga, and K. L. Oub, "Region of interest detection and evaluation in functional near infrared spectroscopy," *J. Near Infrared Spectrosc.*, vol. 24, no. 4, pp. 317–326, 2016, doi: 10.1255/jnirs.1239.

[24] I. Kovelman, M. H. Shalinsky, M. S. Berens, and L. A. Petitto, "Shining new light on the brain's 'bilingual signature': A functional Near Infrared Spectroscopy investigation of semantic processing," *Neuroimage*, vol. 39, no. 3, pp. 1457–1471, 2008, doi: 10.1016/j.neuroimage.2007.10.017.

[25] R. Li, T. Potter, W. Huang, and Y. Zhang, "Enhancing performance of a hybrid EEG-fNIRS system using channel selection and early temporal features," *Front. Hum. Neurosci.*, vol. 11, no. September, pp. 1–11, 2017, doi: 10.3389/fnhum.2017.00462.

[26] J. Kwon, J. Shin, and C. H. Im, "Toward a compact hybrid brain-computer interface (BCI): Performance evaluation of multi-class hybrid EEG-fNIRS BCIs with limited number of channels," *PLoS One*, vol. 15, no. 3, pp. 1–14, 2020, doi: 10.1371/journal.pone.0230491.

[27] S. Ge *et al.*, "A Brain-Computer Interface Based on a Few-Channel EEG-fNIRS Bimodal System," *IEEE Access*, vol. 5, pp. 208–218, 2017, doi: 10.1109/ACCESS.2016.2637409.

[28] X.-S. Hu, K.-S. Hong, and S. S. Ge, "Reduction of trial-to-trial variability in functional near-infrared spectroscopy signals by accounting for resting-state functional connectivity," *J. Biomed. Opt.*, vol. 18, no. 1, p. 017003, 2013, doi: 10.1117/1.jbo.18.1.017003.

[29] S. J. Bak, J. Park, J. Shin, and J. Jeong, "Open-access fNIRS dataset for classification of unilateral finger- and foot-tapping," *Electron.*, vol. 8, no. 12, pp. 1–12, 2019, doi: 10.3390/electronics8121486.

[30] A. Vinciarelli, *Introduction: Social signal processing*. 2017.

[31] K.-S. Hong and H.-D. Nguyen, "State-space models of impulse hemodynamic responses over motor, somatosensory, and visual cortices," *Biomed. Opt. Express*, vol. 5, no. 6, p. 1778, 2014, doi: 10.1364/boe.5.001778.

[32] Z. Y. Shan *et al.*, "Modeling of the hemodynamic responses in block design fMRI studies," *J. Cereb. Blood Flow Metab.*, vol. 34, no. 2, pp. 316–324, 2014, doi: 10.1038/jcbfm.2013.200.

[33] M. A. Lindquist, J. Meng Loh, L. Y. Atlas, and T. D. Wager, "Modeling the hemodynamic response function in fMRI: Efficiency, bias and mis-modeling," *Neuroimage*, vol. 45, no. 1, pp. S187–S198, Mar. 2009, doi: 10.1016/j.neuroimage.2008.10.065.

[34] A. F. Abdelnour and T. Huppert, "Real-time imaging of human brain function by near-infrared spectroscopy using an adaptive general linear model," *Neuroimage*, vol. 46, no. 1, pp. 133–143, 2009, doi: 10.1016/j.neuroimage.2009.01.033.

[35] N. Naseer and K.-S. Hong, "Classification of functional near-infrared spectroscopy signals corresponding to the right- and left-wrist motor imagery for development of a brain–computer interface," *Neurosci. Lett.*, vol. 553, pp. 84–89, Oct. 2013, doi: 10.1016/j.neulet.2013.08.021.

[36] L. C. Schudlo and T. Chau, "Dynamic topographical pattern classification of multichannel prefrontal NIRS signals: II. Online differentiation of mental arithmetic and rest," *J. Neural Eng.*, vol. 11, no. 1, p. 016003, Feb. 2014, doi: 10.1088/1741-2560/11/1/016003.

[37] N. Naseer and K. S. Hong, "Decoding answers to four-choice questions using functional near infrared spectroscopy," *J. Near Infrared Spectrosc.*, vol. 23, no. 1, pp. 23–31, 2015, doi: 10.1255/jnirs.1145.

[38] N. Naseer, F. M. Noori, N. K. Qureshi, and K.-S. Hong, "Determining Optimal Feature-Combination for LDA Classification of Functional Near-Infrared Spectroscopy Signals in

Brain-Computer Interface Application," *Front. Hum. Neurosci.*, vol. 10, May 2016, doi: 10.3389/fnhum.2016.00237.

[39] N. K. Qureshi, N. Naseer, F. M. Noori, H. Nazeer, R. A. Khan, and S. Saleem, "Enhancing Classification Performance of Functional Near-Infrared Spectroscopy- Brain–Computer Interface Using Adaptive Estimation of General Linear Model Coefficients," *Front. Neurorobot.*, vol. 11, Jul. 2017, doi: 10.3389/fnbot.2017.00033.

[40] F. M. Noori, N. Naseer, N. K. Qureshi, H. Nazeer, and R. A. Khan, "Optimal feature selection from fNIRS signals using genetic algorithms for BCI," *Neurosci. Lett.*, vol. 647, pp. 61–66, Apr. 2017, doi: 10.1016/j.neulet.2017.03.013.

[41] H. Nazeer *et al.*, "Enhancing classification accuracy of fNIRS-BCI using features acquired from vector-based phase analysis," *J. Neural Eng.*, vol. 17, no. 5, p. 056025, Oct. 2020, doi: 10.1088/1741-2552/abb417.

[42] N. Naseer, N. K. Qureshi, F. M. Noori, and K.-S. Hong, "Analysis of Different Classification Techniques for Two-Class Functional Near-Infrared Spectroscopy-Based Brain-Computer Interface," *Comput. Intell. Neurosci.*, vol. 2016, pp. 1–11, 2016, doi: 10.1155/2016/5480760.

[43] B. Abibullaev and J. An, "Classification of frontal cortex haemodynamic responses during cognitive tasks using wavelet transforms and machine learning algorithms," *Med. Eng. Phys.*, vol. 34, no. 10, pp. 1394–1410, Dec. 2012, doi: 10.1016/j.medengphy.2012.01.002.

[44] N. Naseer, M. J. Hong, and K.-S. Hong, "Online binary decision decoding using functional near-infrared spectroscopy for the development of brain–computer interface," *Exp. Brain Res.*, vol. 232, no. 2, pp. 555–564, Feb. 2014, doi: 10.1007/s00221-013-3764-1.

[45] N. Thanh Hai, N. Q. Cuong, T. Q. Dang Khoa, and V. Van Toi, "Temporal hemodynamic classification of two hands tapping using functional near—infrared spectroscopy," *Front. Hum. Neurosci.*, vol. 7, 2013, doi: 10.3389/fnhum.2013.00516.

[46] F. Al-Shargie, M. Kiguchi, N. Badruddin, S. C. Dass, A. F. M. Hani, and T. B. Tang, "Mental stress assessment using simultaneous measurement of EEG and fNIRS," *Biomed. Opt. Express*, vol. 7, no. 10, p. 3882, 2016, doi: 10.1364/boe.7.003882.